ISSN 0038-0946, Solar System Research, 2008, Vol. 42, No. 4, pp. 296–318. © Pleiades Publishing, Inc., 2008.
Original Russian Text © V.A. Avdyushev, M.A. Ban'shikova, 2008, published in Astronomicheskii Vestnik, 2008, Vol. 42, No. 4, pp. 317–340.

Determination of the Orbits of Inner Jupiter Satellites

V. A. Avdyushev and M. A. Ban'shikova

Scientific Research Institute of Applied Mathematics and Mechanics, Tomsk State University, Tomsk, Russia

Received June 29, 2007

Abstract—Some problems in determining the orbits of inner satellites associated with the complex behavior of the target function, which is strongly ravine and which possesses multiple minima in the case of the satellite orbit is determined based on fragmentary observations distributed over a rather long time interval, are studied. These peculiarities of the inverse problems are considered by the example of the dynamics of the inner Jupiter satellites: Amalthea, Thebe, Adrastea, and Metis. Numerical models of the satellite motions whose parameters were determined based on ground-based observations available at the moment to date have been constructed. A composite approach has been proposed for the effective search for minima of the target function. The approach allows one to obtain the respective evaluations of the orbital parameters only for several tens of iterations even in the case of very rough initial approximations. If two groups of observations are available (Adrastea), a formal minimization of the target function is shown to give a solution set, which is the best solution from the point of view of representation of the orbital motion, which is impossible to choose. Other estimates are given characterizing the specific nature of the inverse problems.

PACS: 95.10.Ce, 96.30.L-, 95.10.Eg, 91.10.Sp

DOI: 10.1134/S0038094608040035

1. INTRODUCTION

One of the key difficulties in determining the orbit of any inner satellite is attributed to its quick motion around a planet: the frequency of the satellite revolution is so high that, during one year, it makes nearly a thousand rotations or even more. This peculiarity of motion leads to the fact that the target function in inverse problems minimized over orbital parameters has a strongly ravine structure that results in ill conditionality of the quadratic matrix which approximates the target function. In addition, it is known from the optimization theory that the minimization of the ravine functions is very difficult and demands special approaches. When conventional methods of the Gauss–Newton type are used to solve such problems, the iterative schemes of these methods converge badly and have small convergence domains; in fact, their application is possible only at good initial approximations.

Another difficulty is connected with the ambiguity of determining a satellite orbit that takes place when the orbital parameters are determined based on several groups of observations distributed over a long time interval. In this case, the target function can have many equipollent minima and it is difficult to single out the one corresponding to the best orbit parameter estimates. Thus, even if the iteration scheme converges, the practical value of the orbit calculated can still be doubtful.

The present paper considers the peculiarities of the inverse problems based on the data on inner Jupiter satellites: Amalthea (J5), Thebe (J14), Adrastea (J15), and Metis (J16).

The first observers of Amalthea, Thebe, Adrastea, and Metis (Barnard, 1892; Jewitt, et.al.,1979; Synnott, 1984) made attempts to determine their orbital elements based on a few observations. Each new observation encouraged researchers to make successive adjustments to the satellite orbits. Thus, the orbit of the fifth Jupiter satellite discovered as long ago as in 1892 and having been observed for more than a century has been studied better than the orbits of the other three satellites, which were only discovered in 1979. The satellite Thebe, contrary to Adrastea and Metis, has a wider range of observations whose processing does not cause any problems and its orbit has been reliably determined. Along with it, the last two satellites have been observed so rarely that their observations during a rather long time period are distributed only over a few groups. Thus, the processing of these observation data aimed at correcting the orbit parameters is connected to the above difficulties.

Nearby satellites move inside the orbits of Galilean satellites along almost circular Jovian equatorial orbits at the distance from Jupiter of 1.8–3.1 times its radii. Due to the extreme proximity of the satellites to Jupiter, their motion is subjected to the powerful gravitational effect of the massive planet and, thus, the frequencies of the satellite revolutions are very high and the periods corresponding to them lie within the range of 0.3–0.7 days.

The first models of Almatheaís motion were quite simple and took into account only first-order perturbations from Jupiter's oblateness (Tisserand, 1893; Cohn, 1897). Later, researchers began to use kinematic models using the formulas of the precessing Keplerian

ellipses (Van Woerkom, 1950; Sudbury, 1969; Jacobson, 1994). Despite the simplicity of these models, they represent Amaltheaís motion rather well (even in keeping with the accuracy of modern observations) and, thus, continue to be used today to process satellite observations (Jacobson, 1994). However, it should be noted that Sudbury (1969), using the model of the precessing ellipses, failed to unite early observations with a 30-year time gap within one system of orbit parameters. Hypotheses explaining the reason for this failure attribute it to the imperfection of the model used have been set up (Sudbury, 1969; Pascu, 1977). Nevertheless, in our opinion, the most probable reason for this failure lies in the characteristic peculiarity of processing satellite observations which we will consider further in this paper. In addition, it should be noted that Jacobson (1994) managed to overcome this difficulty without resorting to more complex models. Attempts have been made to construct dynamic models based on highly accurate theories of Amaltheaís motion (Kirushenkov, 1969; Arazov, 1972; Breiter, 1996), which are known to not have found wide dissemination in astronomy practice. The analytical theories at present seem to give such an excessively high accuracy (relative to the accuracy of observations) that the models based on them are not in demand. As for satellites such as Thebe, Adrastea, and Metis, the precessing ellipses are used, as a rule, to interpret their motions.

In the present paper, we turn to the numerical integration of satellite orbits (Banshíikova and Avdyushev, 2006), where, for each satellite, the components of its initial dynamic state vector in the phase space of the rectangular coordinates and velocities serve as determined parameters. The numerical models are based on the high-accuracy differential equations of motion which take into account the main gravitational forces as well as the relativistic effects. Like other authors, we determine the orbital parameters in the framework of the least-squares problem based on the available ground-based observations of the satellites; however, to efficiently seek a solution to the problem, we apply a combined approach comprising well-known iteration methods of Gauss and Newton and a gradient descent together with a so-called projection method. In addition, the minimized target functions of the problem were studied with the intent of finding the plurality of the minima and to consider if the corresponding estimates of the orbital parameter are adequate for describing the satellite motions.

THE PROBLEM OF AMBIGUOUS ORBIT DETERMINATION

Let N positions $\mathbf{p}_i^{\mathrm{O}}$ of a celestial body be known at time moments t_i ($i = 1, \ldots, N$); as well, the orbital motion of the object is described by the model

$$\mathbf{p}^{\mathrm{C}} = \mathbf{p}^{\mathrm{C}}(t, \mathbf{q}, E), \quad E = n(t - t_0) + E_0, \tag{1}$$

where $\mathbf{q}$ are the orbital parameters unambiguously determining the trajectory of the celestial body, E is the fast variable, n is the frequency, and E_0 is the variable E in the epoch t_0. Here, $\mathbf{p}^{\mathrm{C}}$ is the 2π periodic over E, i.e., $\mathbf{p}^{\mathrm{C}}(t, \mathbf{q}, E) = \mathbf{p}^{\mathrm{C}}(t, \mathbf{q}, E + 2\pi)$.

Meanwhile, we assume that the parameters $\mathbf{q}$ do not depend on n and consider the squares of distances $\rho_i^2 = \rho^2(\mathbf{p}_i^{\mathrm{O}}, \mathbf{p}_i^{\mathrm{C}})$ between the positions $\mathbf{p}_i^{\mathrm{O}}$ and $\mathbf{p}_i^{\mathrm{C}}$ as functions of n: $\rho_i^2 = \rho_i^2(n)$. It is not difficult to see that the functions ρ_i^2 are periodic over n with corresponding periods $2\pi/(t_i - t_0)$. Therefore, it is evident that the root-mean-square value

$$\sigma^2 = \frac{1}{N}\sum_{i=1}^{N} \rho_i^2 \tag{2}$$

will have an infinite set of minima along n. Thus, the minimization of σ^2 over n will give a set of solutions, only one of which corresponds to the true frequency $\bar{n}$.

The orbits of the inner satellites can also be represented in form (1) where, however, some $\mathbf{q}$ parameters (such as, e.g., the semimajor axis or the focal parameter) are directly linked with the frequency n. Thus, generally speaking, ρ_i^2 turns out to not be periodic over n. Nevertheless, at large enough values of $t_i - t_0$, the functions ρ_i^2 in the neighborhood of the true frequency $\bar{n}$ will be very close to the above periodic components and, as a result, the problem of minima plurality for σ^2 will take place here as well.

A peculiarity in the behavior of σ^2 with regard to n reveals the genesis of the solution set problem, which can occur in the inverse problems of the inner satellite dynamics. Indeed, in practice, the orbital parameters of the satellites are determined, as a rule, from the condition of reaching the minimum by a function similar to (2), which expresses a degree of the proximity of the observed and modeled positions of the object in space $\mathbf{p}$. At least one of the parameters is sure to be associated with the frequency n, but it is this very circumstance that leads to an ambiguous definition of the satellite orbit.

Let us consider the problem of the solution plurality in greater detail using the example of the circular problem, where we can easily obtain obvious and, at the same time, practically useful results allowing one to evaluate the full importance of the problem considered.

CIRCULAR PROBLEM

A circular orbit in a complex plane can be represented as

$$x = ae^{iE}, \quad E = n(t - t_0) + E_0, \quad n = \sqrt{\mu/a^3}, \tag{3}$$

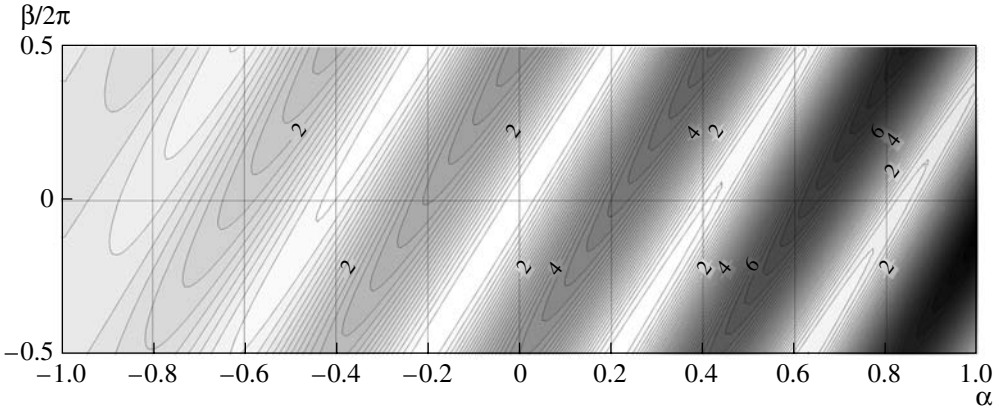

Fig. 1. Behavior of function $f = \alpha^2 + 2(1 + \alpha)(1 - \cos\varphi)$ at $\lambda = 10$.

where x is the position of the point, a is the orbit radius (the semimajor axis), E is the fast phase (anomaly), n is the revolution frequency (mean motion), t is the time, E_0 is the phase at the initial time moment t_0, and μ is the gravitational parameter.

Let us consider a family of orbits (3) and estimate the difference between x and the $\bar{x}$ positions on the orbits (a, E_0) and $((\bar{a}, \bar{E}_0))$, respectively. According to (3), the difference δx is easily transformed into

$$\begin{aligned}\delta x &= x(t, a, E_0) - \bar{x}(t, \bar{a}, \bar{E}_0) \\ &= \bar{a}e^{iE}[1 + \alpha - e^{-i(\lambda\nu + \beta)}],\end{aligned} \tag{4}$$

where $\alpha = (a - \bar{a})/\bar{a}$; $\beta = E_0 - \bar{E}_0$; $\nu = (n - \bar{n})/\bar{n}$, and $\lambda = \bar{n}(t - t_0)$. Assuming that $\alpha \ll 1$ with an accuracy up to the first order of smallness, we will have an estimate $2\nu = -3\alpha$. Then, in accordance with (4), the square of δx will be

$$\begin{aligned}|\delta x|^2 &= \bar{a}^2[\alpha^2 + 2(1 + \alpha)(1 - \cos\varphi)], \\ \varphi &= \frac{3}{2}\lambda\alpha - \beta.\end{aligned} \tag{5}$$

The behavior of $|\delta x|^2$ at small α is thus seen to be mainly determined by the function

$$f = \alpha^2 + 2(1 + \alpha)(1 - \cos\varphi). \tag{6}$$

Figure 1 gives the behavior of the function f versus α and β at $\lambda = 10$. The surface geometry specified by f is seen to have a ravine structure. Here, note that an increase in λ leads to an increase in the ravine shape of f.

Now, assume that the solution of $\bar{x}$ represents the observed positions of the celestial object on a complex plane at certain moments t_i, and set the problem of finding such values of the α and β parameters, which would give the minimum of the target function:

$$\sigma^2 = \frac{1}{N}\sum_{i=1}^{N}|\delta x|_i^2, \tag{7}$$

where N is the number of observations. Let us consider the observations for which $|\lambda| \gg 0$. Then, the behavior of σ^2 versus α and β will be mainly determined by trigonometric components. Thus, we must be interested, in fact, in the function having the type

$$f_{\cos} = 1 - \frac{1}{N}\sum_{i=1}^{N}\cos\varphi_i, \quad \varphi_i = \frac{3}{2}\lambda_i\alpha - \beta. \tag{8}$$

Note that, at a enough large λ_i differing by magnitudes less than on the order of α^{-1}, the function will behave itself as one trigonometric component:

$$f_{\cos} \approx 1 - \cos\varphi,$$

where one of the values of λ_i is chosen as λ. Consequently, all observations with such λ_i can be grouped and considered as one observation. If there are several such groups, the function behavior can be represented as

$$\begin{aligned}f_{\cos} \approx F \equiv 1 - \sum_{j=1}^{M} k_j\cos(\omega_j\alpha - \beta), \\ k_j = \frac{N_j}{N}, \quad \omega_j = \frac{3}{2}\lambda_j,\end{aligned} \tag{9}$$

where M is the number of groups, k_j is the weight of the j group determined by the number of observations in the group N_j, and λ_j is one of the values of the $\lambda\, j$ group. Thus, weíll assume that $\lambda_1 \ll \lambda_2 \ll \ldots \ll \lambda_M$.

Using the known trigonometric identities, F can be rewritten as

$$F = 1 - A\cos(\beta + \psi),$$
$$\text{where } A = \sqrt{c^2 + s^2}, \quad \psi = \arctan(s/c), \tag{10}$$
$$c = \sum_{j=1}^{M} k_j \cos(\omega_j \alpha), \quad s = \sum_{j=1}^{M} k_j \sin(\omega_j \alpha).$$

From this, it follows that F is 2π periodical over β and, if α is fixed, it has the only minimum at the half-space interval $(\beta_0 - \pi, \beta_0 + \pi)$ for any $\beta_0 \in (-\infty, +\infty)$. Consequently, the area of investigation of F over β can be reduced to any half-space 2π long.

Let us introduce the characteristic

$$\Phi(\alpha) = \min_{\beta \in (-\pi, +\pi]} F(\alpha, \beta), \tag{11}$$

which is peculiar, because it does not depend on the choice of the initial epoch. Really, the change in the initial epoch $t_0 \longrightarrow t_0 + \Delta t$ in accordance with (9) leads to a transformation of the shift along β:

$$F(\alpha, \beta)|_{t_0 + \Delta t} = F(\alpha, \beta + \Delta\beta)|_{t_0}, \quad \text{where } \Delta\beta \propto \alpha \Delta t.$$

In view of the above properties of F,

$$\min_{\beta \in (-\pi, +\pi]} F(\alpha, \beta)|_{t_0 + \Delta t} = \min_{\beta \in (-\pi, +\pi]} F(\alpha, \beta + \Delta\beta)|_{t_0} = \Phi(\alpha).$$

Note that the characteristic $\Phi(\alpha)$ is a single-valued function of α and, thus, the minima of $\Phi(\alpha)$ over α will unambiguously correspond to the minima of $F(\alpha, \beta)$ over α and $\beta \in (-\pi, +\pi)$. From (10), we can easily get the formula for Φ:

$$\Phi(\alpha) = 1 - A(\alpha). \tag{12}$$

It is not difficult to see that the coefficients c and s can be represented as

$$c = \frac{1}{N}\sum_{i=1}^{N} \cos(\omega_i \alpha), \quad s = \frac{1}{N}\sum_{i=1}^{N} \sin(\omega_i \alpha).$$

It should be specially noted that the surface geometry assigned by the function $F(\alpha, \beta)$ in the neighborhood of the minima is strongly ravine. It is mainly stipulated by large ω_j. Therefore, with an accuracy up to second-order small values, the behavior of $F(\alpha, \beta)$ in the neighborhood of a trivial minimum $\alpha = \beta = 0$ can be represented by the function

$$Q(\alpha, \beta) = \frac{1}{2}(\kappa_{11}\alpha^2 + 2\kappa_{12}\alpha\beta + \kappa_{22}\beta^2), \tag{13}$$

where

$$\kappa_{11} = \sum_{j=1}^{M} k_j \omega_j^2, \quad \kappa_{12} = -\sum_{j=1}^{M} k_j \omega_j, \quad \kappa_{22} = 1. \tag{14}$$

The equation $Q(\alpha, \beta) = \text{const}$ describes a certain ellipse in the plane (α, β) with its center in the trivial minimum. It is known from the analytical geometry that the square of the ratio of C of the major ellipse semiaxis to the minor one can be represented as

$$C^2 = \frac{\kappa_{11} + \kappa + \kappa_{22}}{\kappa_{11} - \kappa + \kappa_{22}},$$
$$\text{where } \kappa = \sqrt{4\kappa_{12}^2 + (\kappa_{11} - \kappa_{22})^2}.$$

From here, taking (14) into account, for enough large ω_j, weíll have

$$C^2 \sim \kappa_{11}. \tag{15}$$

However, the ravinity can be slightly reduced by choosing the initial epoch t_0. According to approximate estimator (15), the ration C^2 will be close to minimal at

$$t_0 = \sum_{j=1}^{M} k_j t_j,$$

where t_j is one of the observation epochs of the j group. Hence, to decrease the ravanity of $F(\alpha, \beta)$, the simple average of all observation epochs should be taken as the initial epoch. Chernitsov (1975) made first mention of this. In addition, such a choice for the initial epoch reduces the quadratic form of (13) to a canonical one as κ_{12} vanishes.

To analyze the function F, it is more convenient to represent it as

$$F = 1 - \sum_{j=1}^{M} k_j \cos((l_j - l_0)\zeta - \beta), \tag{16}$$

$$\zeta = \frac{3}{2}\alpha(\lambda_M - \lambda_1),$$

$$l_j = \frac{\lambda_j - \lambda_1}{\lambda_M - \lambda_1} \quad (j = 0, 1, \ldots, M), \quad \lambda_0 = 0.$$

Here, l_0 and $l_j \in [0, 1]$ $(j = 1, 2, \ldots, M)$ are the time distribution of the initial epoch and the observation group with regard to the first group, respectively.

Let us consider two groups of observations ($M = 2$) of the same weight ($k = 1/2$). This case corresponds to the distribution of the ground-based observations of the inner Jupiter satellite Adrastea (J15) currently available. Figure 2 gives the behavior of the function $F(\zeta, \beta)$ (16) at different $l_0 \in [0, 1/2]$.

It is evident from the figure that variations of the parameter l_0, i.e., variations of the initial epoch, result in the shift of the geometry of the surface $F(\zeta, \beta)$ along β. Thus, a degree of the surface ravinity changes as well: thus, ravines at $l_0 = 0$ (the initial epoch in the neighborhood of the first observation group epochs) are visibly more elongated than those at $l_0 = 1/2$ (the initial epoch lies in the center of the time interval considered).

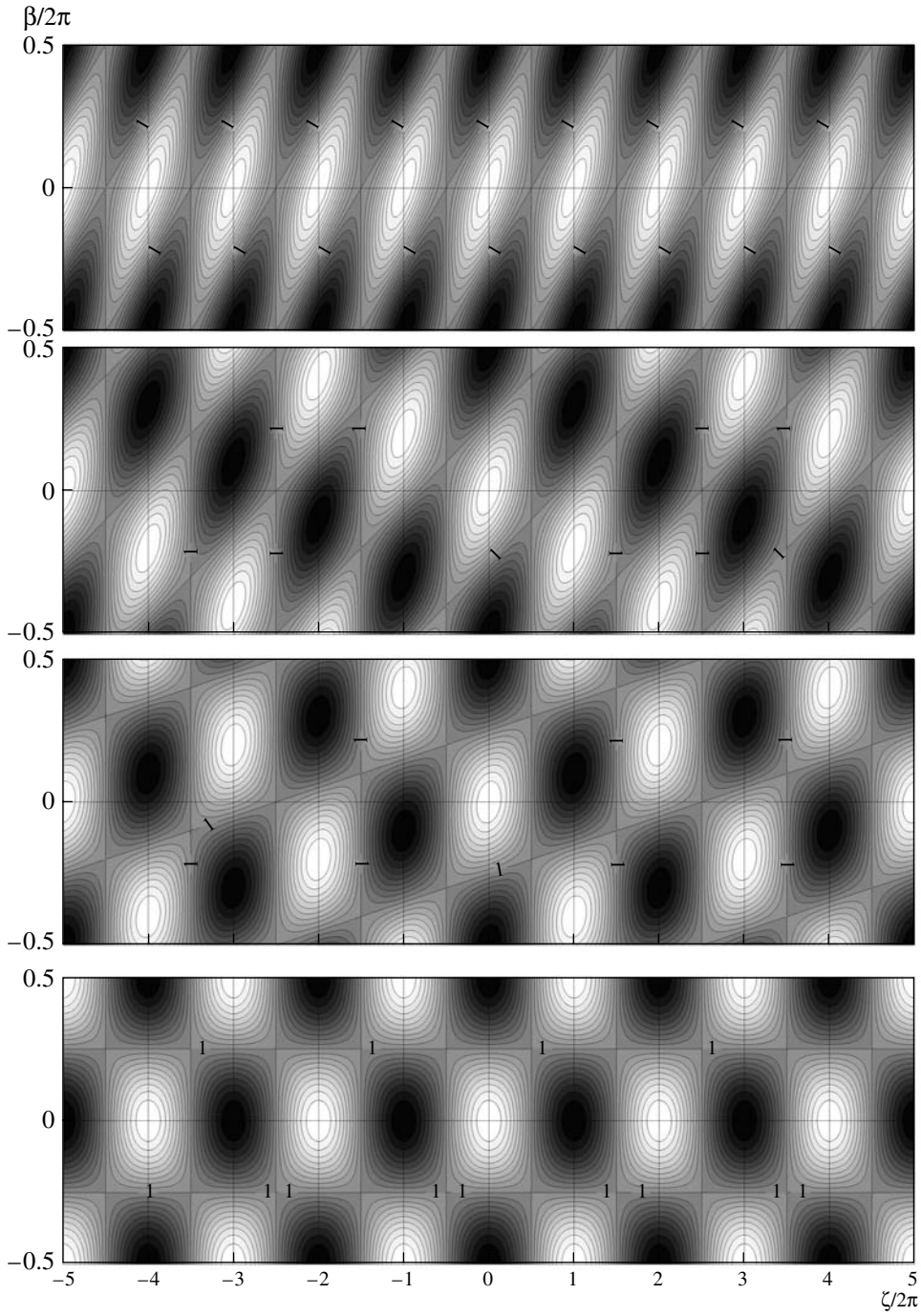

Fig. 2. Behavior of $F(\zeta, \beta)$ for two groups of observations of the same weight and different l_0: 0.0, 0.2, 0.4, and 0.5 (from the top down, respectively) (Adrastea).

These results confirm our conclusions above concerning the behavior of the function F. At the same time, the characteristic Φ remains constant for all l_0) (Fig.3). In the general case, at different $k_1 = k$ and $k_2 = 1 - k$,where $k \in (0,1)$, the characteristics of Φ in accordance with (10) and (12) can be represented as

$$\Phi = 1 - \sqrt{1 - 2k(1-k)(1-\cos\zeta)}.$$

From the presence of a trigonometric component in the characteristics Φ it follows that for any two groups of observations there is a manifold of equipollent minima F corresponding to $\zeta = 2\pi m$ or

$$\alpha = \frac{4\pi m}{3(\lambda_M - \lambda_1)} = \frac{2}{3}\frac{m}{R}, \qquad (17)$$

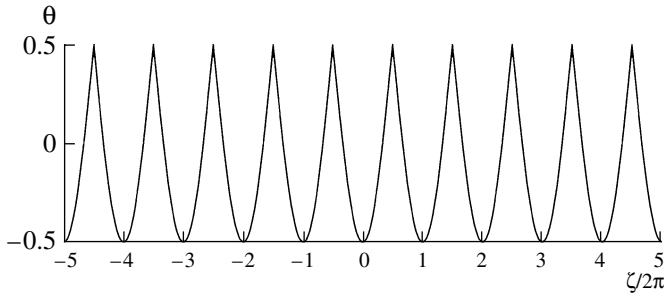

Fig. 3. Behavior of $\Phi(\zeta)$ for two groups of observations of the same weight (Adrastea).

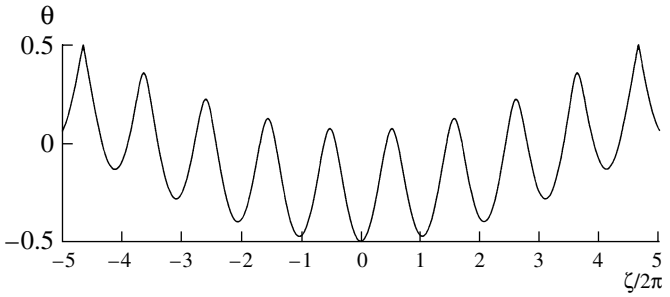

Fig. 4. Behavior of $\Phi(\zeta)$ for three groups of observations (Metis).

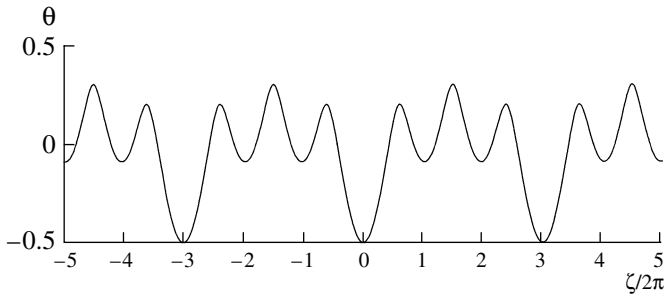

Fig. 5. Behavior of $\Phi(\zeta)$ for three groups of observations with resonant distribution: $l_1 = 0$, $l_2 = 2/3$, and $l_3 = 1$.

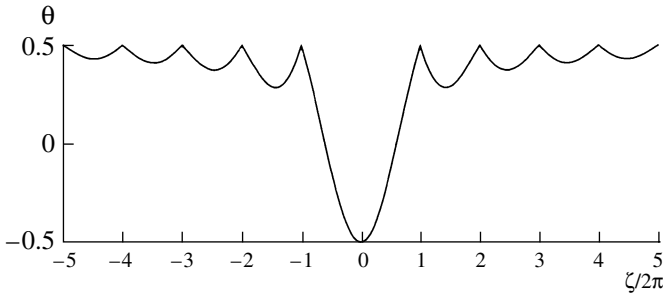

Fig. 6. Behavior of $\Phi^\infty(\zeta)$.

where m are integers and R is the number of revolutions during $\lambda_M - \lambda_1$.

The case of three groups of observations (even if they are equilibrium) is more difficult to investigate. Thus, let us consider only a particular case corresponding to the distribution of ground-based observations of Metis (J16): $k_1 = 0.28$, $k_2 = 0.16$, $k_3 = 0.56$, $l_1 = 0$, $l_2 = 0.92$, $l_3 = 1$.

The characteristic Φ (Fig.4), as it is in case of two observation groups, has a manifold of minima. Strictly speaking, a distinctive feature of the characteristics for three groups is the fact that these minima are not equipollent and in the considered variation interval ζ there is an explicit minimum corresponding to the true solution.

However, if the distribution of observation groups is such that the values of l_j satisfy the resonance relation of the type

$$\sum_{j=2}^{M} m_j l_j = 0, \qquad (18)$$

where $m_j \neq 0$ are the integers, a manifold of absolute minima F can exist.

The higher the density of the minima distributions along ζ, the lower the resonance order and the smaller the values of m_j. An example of the observation group resonance distributions for $M = 3$ is given in Fig. 5, where the same weights as those in the Metis observations are used. Here, we have the resonance $l_2/l_3 = 2/3$, which leads to a plurality of the absolute minima with the interval 6π uniformly distributed along ζ. Evidently, due to the increase in resonance order (18), the increase in the number of fragmentary M groups will decrease the density of the absolute minima.

The case of the multiple uniformly distributed and equilibrium groups is also of interest. It is not difficult to show that if M is large enough

$$F \approx F^\infty \equiv F|_{M\to\infty}$$

$$= 1 - \frac{1}{\zeta}[\sin((1-l_0)\zeta - \beta) - \sin(-l_0\zeta - \beta)].$$

Then,

$$\Phi \approx \Phi^\infty \equiv \Phi|_{M\to\infty} = 1 - \left|\frac{2}{\zeta}\sin\frac{\zeta}{2}\right|.$$

The behavior of Φ^∞ is given in Fig. 6, where we see that, even in the case of the dense distribution of the observation groups, the function F will also have a set of minima among which only one absolute minimum is prominent.

From Fig. 6 we can retrieve other information, which is also useful for gaining practical knowledge on the target function behavior. We assume that to minimize the target function σ^2, we use a numerical (iteration) method of the Gauss–Newton type. Then, the plot in the figure givesmarginal values of the maximum pos-

sible ζ, at which the iteration method can still be converged to a trivial minimum. If the initial approximation of the orbital parameters is such that $|\zeta| > 2\pi$ or, otherwise, the error in the semimajor axis is so large that

$$|\alpha| > \frac{2}{3}\frac{1}{R},$$

then, the method wonít be convergent even in the case of a dense time distribution for the observation epochs. Evidently, the interval of convergence (overα) to a trivial minimum will only become shorter during the thinning of the observation data (see, e.g., Figs. 3–5). We think that this possible reason for Sudburryís failure (1969) in his attempt to find a uniform system of Amaltheaís elements based on two groups of observations separated by a 30-year-long time interval. The initial parameter estimates were evidently so rough that they simply didnít fall into the area of the minimization method convergence.

In spite of the fact that at $|\lambda_j| \gg 0$ the target function σ^2 (7) is rather well represented by its trigonometric component $f_{\cos}$ (8); the first one, contrary to the latter, will always have only one absolute minimum at $\alpha = \beta = 0$ corresponding to the intrinsic solution of $\bar{x}$, where the target function vanishes. It is attributed to the fact that σ^2 has a quadratic term α^2. In other minima, the target function takes on different (nonzero) values. Thus, in our case, the condition of the least value of σ^2 at the set of all minima can be taken as the criterion of the true solution x (according to observations of $\bar{x}$).

Note, however, that, for near-resonance distributions of l_j, only the minima at which the function σ^2 is nearly zero can take place. Thus, the higher the density of their occurrence, the lower the order of their commensurability. Let us call these minima as pseudotrivial.

In addition, it should be noted that, if a is fixed and n (independent of a) and E_0 are considered as the parameters to be estimated, then the function σ^2 will be similar to $f_{\cos}$ with all its peculiarities, but, in this case, with regard to ν (4) and β.

By now, we have assumed that the observations represented by the solution $\bar{x}$, are accurate, but, in case of (random) errors in $\delta\bar{x}$, the function σ^2, generally speaking, will not take on zero values and, in addition, the most plausible solution in the neighborhood of $\alpha = \beta = 0$ cannot give an absolute minimum: due to errors, the status of an absolute minimum can move to one of the pseudotrivial minima. Consequently, in this case, the condition of the lower-range value of σ^2 cannot be taken as a criterion of the maximum likelihood.

Of particular interest is the case when in anomaly E there are secular errors $\lambda^* = n^*(t - t_0)$, which manifest themselves in practice as the results of unmodeled effects, in particular, when some force models are either ignored or simplified. It is easy to show that the effect of secular errors λ^* leads to a shift in function $f_{\cos}$ (8) along α, while corresponding values of the function maxima are preserved. Thus, the parameter φ is transformed to the form

$$\varphi = \lambda\left(\frac{3}{2}\alpha - \frac{n^*}{\bar{n}}\right) - \beta.$$

It follows, for example, that, even if a simplified (rough) and a complicated (a more accurate) model yields the same minima of target function σ^2, it cannot be chosen in favor of the first model because the values of σ^2 determined in the case of α 2 is minimized and will be fundamentally different.

Note, finally, that the set of σ^2 minima will take place only for $M > 1$. In the one group of close-range observations,

$$\min_{\beta \in (-\pi, +\pi]} \sigma^2 = \alpha^2.$$

This implies that the target function for $M = 1$ must have the only minimum at $\alpha = \beta = 0$.

Hence, the target function σ^2 (7) (for $M > 1$) has a set of minima. Thus, when using numerical (iteration) methods for the minimization of σ^2 over a and E_0 (3), the solution obtained will directly depend on the chosen initial approximation. Thus, from among all minima, we cannot always recognize the one corresponding to the true solution to $\bar{x}$. In particular, it can take place when $|\lambda_j| \gg 0$.

THE GAUSS–NEWTON METHOD

Let us have N-observed positions of $\mathbf{p}_i^{\mathrm{O}}$ in the L-dimensional space at time moments t_i ($i = 1, \ldots, N$). It is necessary, based on $\mathbf{p}_i^{\mathrm{O}}$ observations, to determine K orbital parameters of $\mathbf{q}$.

Usually, the determination of $\mathbf{q}$ is reduced to the minimization of the functional

$$S(\mathbf{q}) = \frac{1}{2}\sum_{i=1}^{N} \rho^2(\mathbf{p}_i^{\mathrm{O}}, \mathbf{p}_i^{\mathrm{C}}), \qquad (19)$$

where ρ is the metric in space $\mathbf{p}$, while $\mathbf{p}_i^{\mathrm{C}} = \mathbf{p}^{\mathrm{C}}(t_i, \mathbf{q})$ is the numerical representation of $\mathbf{p}_i^{\mathrm{O}}$ over $\mathbf{q}$ based on the orbital motion modeling. Let us assign the metric as

$$\rho(\mathbf{p}_1, \mathbf{p}_2) = \sqrt{(p_{11} - p_{12})^2 + \ldots + (p_{L1} - p_{L2})^2},$$

where $p_{11}, \ldots, p_{L1}$ and $p_{12}, \ldots, p_{L2}$ are the components of vectors $\mathbf{p}_1$ and $\mathbf{p}_2$, respectively. Then, Eq. (19) can be rewritten as

$$S(\mathbf{q}) = \frac{1}{2}\sum_{i=1}^{L}\sum_{j=1}^{N} (p_{ij}^{\mathrm{O}} - p_{ij}^{\mathrm{C}})^2. \qquad (20)$$

The minimum of functional (20) is found from the necessary condition of the extremum over $\mathbf{q} = (q_1, \ldots, q_K)$:

$$\frac{\partial S}{\partial \mathbf{q}} = -\sum_{i=1}^{L}\sum_{j=1}^{N}(p_{ij}^{O} - p_{ij}^{C})\frac{\partial p_{ij}^{C}}{\partial \mathbf{q}} = \mathbf{0}. \quad (21)$$

To solve system of equations (21) with regard to the parameter $\mathbf{q}$, we turn to iteration methods. According to the Newton iteration scheme, a correction to the current approximation of $\mathbf{q}$ is determined as

$$\Delta\mathbf{q} = -\left(\frac{\partial^2 S}{\partial \mathbf{q}^2}\right)^{-1}\frac{\partial S}{\partial \mathbf{q}}, \quad (22)$$

where $\partial^2 S/\partial \mathbf{q}^2$ is the Hessian matrix:

$$\frac{\partial^2 S}{\partial \mathbf{q}^2} = \sum_{i=1}^{L}\sum_{j=1}^{N}\left[\frac{\partial p_{ij}^{C}}{\partial \mathbf{q}}\frac{\partial p_{ij}^{C}}{\partial \mathbf{q}} - (p_{ij}^{O} - p_{ij}^{C})\frac{\partial^2 p_{ij}^{C}}{\partial \mathbf{q}^2}\right]. \quad (23)$$

In Eq. (22), the initial approximation of $\mathbf{q}$ is usually taken from the preliminary determination of the orbit from several observations within the framework of a two-body problem.

Because it is problematic to calculate the second derivatives in Eq. (22), in practice, these are omitted and, thus, we turn to a so-called Gauss–Newton method which pertains to a wide class of quasi-Newton methods.

Let us introduce the matrix

$$\mathbf{A}_{LN\times K} = \begin{pmatrix} \frac{\partial p_{11}^{C}}{\partial q_1} & \cdots & \frac{\partial p_{11}^{C}}{\partial q_K} \\ \vdots & \ddots & \vdots \\ \frac{\partial p_{L1}^{C}}{\partial q_1} & \cdots & \frac{\partial p_{L1}^{C}}{\partial q_K} \\ \frac{\partial p_{12}^{C}}{\partial q_1} & \cdots & \frac{\partial p_{12}^{C}}{\partial q_K} \\ \vdots & \ddots & \vdots \\ \frac{\partial p_{LN}^{C}}{\partial q_1} & \cdots & \frac{\partial p_{LN}^{C}}{\partial q_K} \end{pmatrix} \quad (24)$$

$$\text{and } \mathbf{B}_{LN\times 1} = \begin{pmatrix} p_{11}^{O} - p_{11}^{C} \\ \vdots \\ p_{L1}^{O} - p_{L1}^{C} \\ p_{12}^{O} - p_{12}^{C} \\ \vdots \\ p_{LN}^{O} - p_{LN}^{C} \end{pmatrix}.$$

Then, correction (22) can be rewritten as

$$\Delta\mathbf{q} = -\mathbf{Q}^{-1}\mathbf{G}, \quad (25)$$

where $\mathbf{Q} = \mathbf{A}^T\mathbf{A}$ is the normal matrix which in the minimum $S(\mathbf{q})$ at rather small discrepancies $\mathbf{B}$ is close to the Hessian matrix, and $\mathbf{G} = -\mathbf{A}^T\mathbf{B}$ is the gradient of the function S over $\mathbf{q}$.

In practice, we observe two angular object coordinates: a right ascension p_1^O and a declination p_2^O. In this case, the distances between the observed and the calculated positions in the coelosphere are computed by the formula

$$\rho(\mathbf{p}_i^O, \mathbf{p}_i^C) = \sqrt{(p_{1i}^O - p_{1i}^C)^2\cos^2 p_{2i}^O + (p_{2i}^O - p_{2i}^C)^2},$$

while the following is considered as a functional of (20):

$$S(\mathbf{q}) = \frac{1}{2}\sum_{i=1}^{N}[(p_{1i}^O - p_{1i}^C)^2\cos^2 p_{2i}^O + (p_{2i}^O - p_{2i}^C)^2]. \quad (26)$$

TWO-BODY PROBLEM

To study the capabilities of the Gauss–Newton method in detail, we first applied it to a simple model based on two-body problem formulas. The model simulated the motion of the satellite Adrastea in the angular coordinate space. As orbital parameters, we took the components of the initial vector of the dynamic state $\mathbf{q} = (\mathbf{x}_0, \dot{\mathbf{x}}_0)$, which were preliminarily obtained from observations using the Laplace method (Escobal, 1965). Here, the parameters $\mathbf{q}$ corresponded to a nearly circular orbit with the semimajor axis $\bar{a} = 8.68 \times 10^{-4}$ AU and the eccentricity $\bar{e} = 0.0161$. Based on the vector $\mathbf{q}$, we modeled observed (accurate) positions of $\mathbf{p}^O = (p_1^O, p_2^O)$ (angular satellite coordinates) at the moment of real observations ($N = 90$) almost identically distributed over the extremities of a 12-year interval. The initial epoch t_0 was taken in the middle of the time interval.

Varying the a and e components and getting different initial approximations of $\mathbf{q}_0$, we determined orbital parameters $\mathbf{q}$ over $\mathbf{p}^O$ according to (25) as applied to (26). Thus, after numerous experiments, we discovered that the iteration process is converged not at all values of $\mathbf{q}_0$, and, even when it converges, the solution is not always true. Hence, the domain of convergence to expected components $\bar{a}$ and $\bar{e}$ is rather small. The reason for the divergence of the iteration process (even at good initial approximations of $\mathbf{q}_0$ providing for small values of the target function) seems to be mainly connected to the strong ravinity and the complex structure of the hypersurface assigned by $S(\mathbf{q})$.

However, the convergence can nearly always be attained by decreasing the values of correction (25), i.e., in accordance with the scheme

$$\Delta\mathbf{q} = -h\mathbf{Q}^{-1}\mathbf{G}, \quad \text{where } h < 1. \quad (27)$$

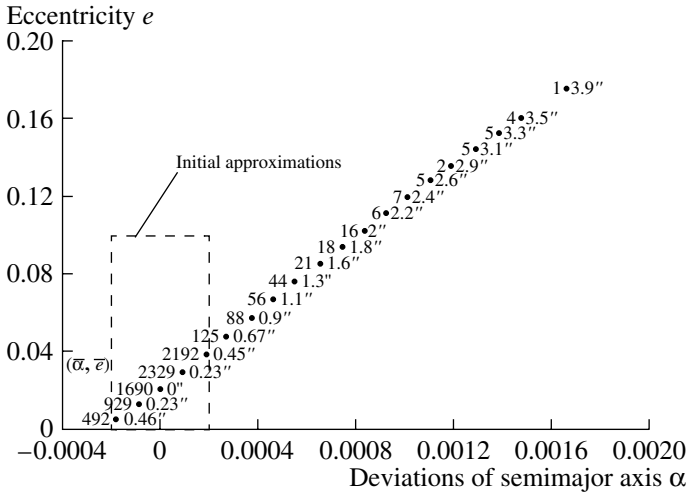

Fig. 7. Set of solutions in the plane (α, *e*).

Figure 7 gives the results obtained for $h = 0.01$. Here, α is the relative deviation of the semimajor axis a from the true value $\bar{a}$, i.e., $a = \bar{a}(1 + \alpha)$. The dots denote the solutions to which the iteration process converged at different initial variations of α and e (inside the rectangle with the dashed line border). The numbers to the left of the dots denote how many times the iteration process converged to a corresponding solution, while the numbers to the right represent the mean-square error $\sigma = \sqrt{S/N}$, obtained in this solution. Here, 2000000 initial approximations were considered and only 0.4% of them converged; the majority of them, in turn, converge to solutions in the domain of variation of the elements.

Thus, the problem considered also has a set of solutions; however, among them, the absolute minimum is given by the solution corresponding to the initial orbital elements $\bar{a}$ and $\bar{e}$. Note that nearly all minima along the axis α are uniformly distributed, the step being $\Delta\alpha \approx 9.23 \times 10^{-5}$. It is easy to check that this distribution is in good agreement with the estimates of (17) for even m. The reason for the absence of minima for odd m lies in the special selection of the initial epoch. Now, let us return to Fig. 2. The lower plot shows that, in the case of a circular problem with the initial epoch lying in the middle of the time interval (as it is in our case), the solutions that yield the criterion problem minima must lie on the orbit at nearly diametrically opposed points. Varying only the semimajor axis and the eccentricity, we practically excluded those initial approximations which could yield the minima corresponding to odd m (17) in the opposite part of the orbit. At the same time, the upper plot in Fig. 2 shows that the choice of the epoch within one group localizes the minima, which is naturally convenient for the search.

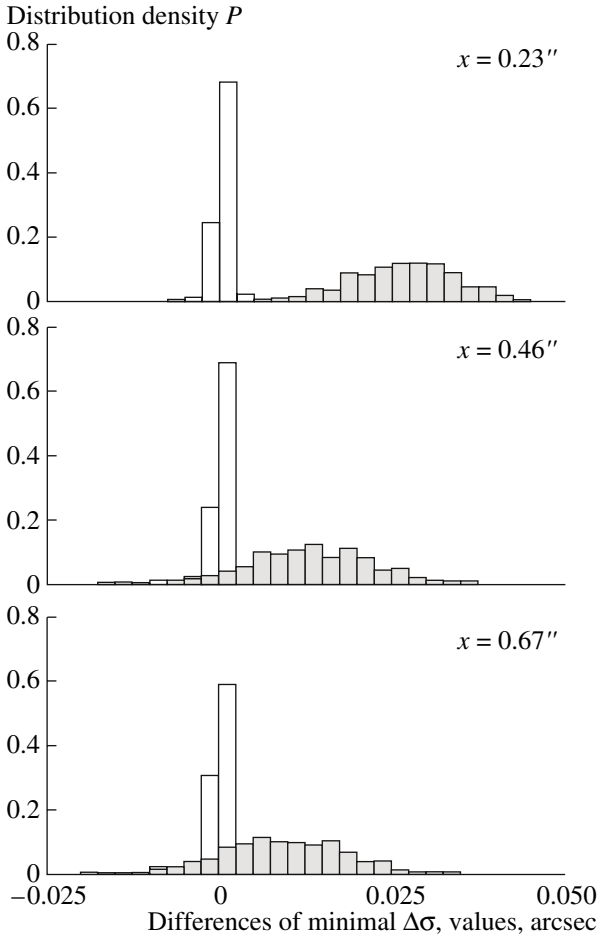

Fig. 8. Probabilistic densities of the differences of minimal Δσ values for different samplings of observation errors with dispersions $s = 0.23''$, $0.46''$, and $0.67''$ (grey for $N = 90$; white for $N = 20$).

Furthermore, since we assume that the modeled observations are free from errors, in the absolute minimum, $\sigma = 0$. In neighboring minima, $\sigma = 0.23''$. Thus, when there are random errors in the observations with the dispersion on the order of a mean-square value, the minimum of σ for the true orbit can be comparable with the neighboring analogs to an extent that it will not be recognized as the minimum corresponding to the true orbit.

Having performed the procedure to determine the orbit for different samples of the normally distributed errors introduced into the modeled observations, we compared the values of the minima for the true orbit with those of one of the neighboring analogs. Figure 8 gives probabilistic densities P for the differences Δσ in cases of three dispersion errors $s = 0.23''$, $0.46''$, and $0.67''$. A positive difference means that the minimum corresponding to the true orbit is smaller than the neighboring one.

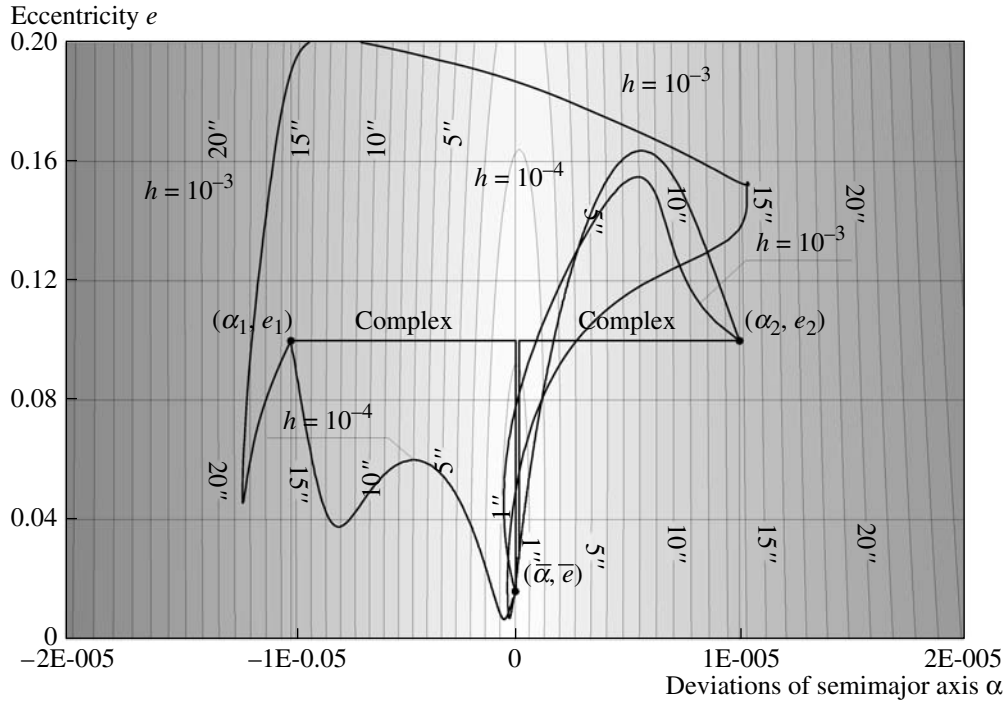

Fig. 9. Convergence of methods (accurate observations, $N = 90$).

In particular, it is evident from the figure that, at rather small errors ($s = 0.23''$), the differences $\Delta\sigma$ take on positive values, where $\Delta\sigma = 0.02$–$0.03''$ is the most probable. Consequently, the parameters returning the smallest minimum can be considered as the best estimates of the true orbital parameters. In contrast to this case, the two other values yield negative differences whose occurrences are comparable with those for the positive differences. This testifies to the fact that, by comparing two neighboring minima, it is impossible to reliably estimate the soundness of the parameters corresponding to them.

It is possible to determine the status of the neighboring minima if we have a great number of observations (which are accurate enough). Otherwise, this undertaking is unreliable. Figure 8 shows the results of the experiments for 20 observation epochs (10 for each group). It is evident that the majority of the differences in all cases ($N = 20$) is concentrated at zero. Hence, the probability of the occurrence of negative differences is rather high.

As mentioned above, the convergence of the Gauss–Newton iteration scheme can be attained if we introduce into it a decreasing multiplier h (27). To get the numerical results, in the previous section, we used $h = 0.01$. However, taking into account the low percent of solution convergence (0.4%), we can assume that, to yield a more consistent parametric estimation of $\mathbf{q}$, by minimizing the target function S, we should choose a significantly smaller multiplier.

We estimated the convergence character and the rate of the Gauss–Newton scheme with different h multipliers using the example of two rather rough initial approximations $\mathbf{q}_{01}$ and $\mathbf{q}_{02}$ corresponding to the parameters $\alpha_1 = -10^{-5}$, $e_1 = 0.1$ and $\alpha_2 = 10^{-5}$, $e_2 = 0.1$. The monitoring of the iteration process was performed in the plane (α, e). The results are shown in Fig. 9. Here, there is also a plot of isolines of S as functions of α and e for true values of other orbital parameters.

In particular, it is evident from the figure that even for $h = 0.001$ successive approximations with the initial $\mathbf{q}_{01}(\alpha_1, e_1)$ are determined in a rather unpredictable way although the iteration process converges. At the same time, a significant decrease in the multiplier ($h = 0.0001$) both for $\mathbf{q}_{01}$ and $\mathbf{q}_{02}$ leads to a desirable relaxation series of approximations. Finally, it should be noted that, at $h = 0.01$, the iteration process diverges in both cases.

In spite of such a simple approach to the convergence problem solution, it is unacceptable for determining the orbits of real inner satellites since, due to the specific nature of the inverse problem, it is associated with a very low convergence rate. Thus, when using a scheme for the iteration process convergence with the multiplier $h = 0.001$ (the coordinate accuracy being 10^{-10} AU), we had to carry out more than 10000 iterations.

GRADIENT DESCENT AND PROJECTION METHOD

With the aim of attaining a rapid convergence of the iteration process, it is possible to use other methods of

calculating $\Delta\mathbf{q}$ corrections together with the Gauss–Newton method. In our case, it is enough to turn to the well-known method of the gradient descent and the so-called projection method (Himmelblau, 1972).

In the gradient descent method, the correction is calculated as (Attetkov, et. al, 2001)

$$\Delta\mathbf{q} = -\frac{\mathbf{G}\cdot\mathbf{G}}{(\mathbf{Q}\mathbf{G})\cdot\mathbf{G}}\mathbf{G}. \quad (28)$$

Here, the point denotes the inner product of the K-dimensional vectors. During the process of the successive use of scheme (28), the approximated solution very quickly (during several iterations) falls down to the bottom of ravine S, but later, extremely slowly reduces to the minimum S. At this stage, one can use the Gauss–Newton method. However, as practice shows, if an approximated solution is very far from the minimum S, scheme (25) will make corrections which are capable of throwing the solution from the domain of the method convergence. However, bad corrections can be improved if we use a priori information on the properties of the orbital motion.

The gravitational field of the planet plays a dominant role in the motion of Jupiterís inner satellites. When modeling, this can be considered as conservative.

Thus, the total energy $H(\mathbf{q})$ determined by the planet attraction will be nearly constant. Taking this property into account, let us impose a limitation on $\Delta\mathbf{q}$: a correction should meet the condition that $H(\mathbf{q}+\Delta\mathbf{q}) = H(\mathbf{q})$, i.e., the approximate solution should remain at one energy level.

For the general case, the imposed limitation determines many corrections; however, it is expedient to use only an orthogonal projection of correction (25) onto the surface $H(\mathbf{q})$. Algorithmically, it is possible to make the following iteration scheme:

$$\Delta\mathbf{q}_{i+1} = \Delta\mathbf{q}_i - \frac{H(\mathbf{q}+\Delta\mathbf{q}_i) - H(\mathbf{q})}{\mathbf{G}_H\cdot\mathbf{G}_H}\mathbf{G}_H \quad (29)$$
$$(i = 0, 1, \ldots),$$

where $\mathbf{G}_H = \partial H/\partial\mathbf{q}$ is the gradient H over $\mathbf{q}$, while $\Delta\mathbf{q}_0$ is determined from (25).

As soon as the approximate solution becomes close enough to the minimum, which is determined by the smallness of $\Delta\mathbf{q}_0$, we stop the minimization of S using Gauss–Newton scheme (25).

A composite approach using iteration schemes (25), (28), and (29) was also tested for initial approximations of $\mathbf{q}_{01}$ and $\mathbf{q}_{02}$. The test results are given in Fig. 9 (complex). The horizontal trajectories, here, correspond to gradient descent (28), while the vertical trajectories correspond to the Gauss–Newton method together with projection scheme (29), where the Keplerian energy was taken as H. Most noteworthy here is the fact that only 27 iterations were needed to reach convergence for the iteration process in both cases.

SATELLITE MOTION MODEL

A numerical model of satellite motion $\mathbf{p}^{\mathrm{C}}$ in the angle coordinate space $\mathbf{p} = (p_1, p_2)$] with regard to a standard Earth equator J2000 can be formally represented as

$$\mathbf{p}^{\mathrm{C}} = \mathbf{p}^{\mathrm{C}}(t, \mathbf{q}^{\mathrm{DT}}) = \mathbf{T}(t, \mathbf{x}(t, \mathbf{q}^{\mathrm{D}}), \mathbf{q}^{\mathrm{T}}). \quad (30)$$

Here, t is the ephemeris time; $\mathbf{q}^{\mathrm{DT}} = (\mathbf{q}^{\mathrm{D}}, \mathbf{q}^{\mathrm{T}})$ is the vector of all model parameters; $\mathbf{T}$ is the transformation of the transition from a Jovian central frame to a topocentric system; $\mathbf{q}^{\mathrm{D}} = (\mathbf{x}_0, \dot{\mathbf{x}}_0, t_0, q_8, \ldots)$, and $\mathbf{q}^{\mathrm{T}}$ are the parametric vectors related to the satellite motion with regard to a Jovian center and that with a coordinate transformation, respectively; $\mathbf{x}$ is the jovicentric position of the satellite; and $\mathbf{x}_0$ and $\dot{\mathbf{x}}_0$ are the vectors of the dynamic satellite state at the initial moment t_0.

Model (30) determines the position of $\mathbf{x}$ through the numerical integration of the differential equations of motion

$$\frac{\mathrm{d}^2\mathbf{x}}{\mathrm{d}t^2} = \mathbf{P}(t, \mathbf{x}, \dot{\mathbf{x}}, \mathbf{q}^{\mathrm{D}}) = \mathbf{P}_{\mathrm{J}} + \mathbf{P}_{\mathrm{G}} + \mathbf{P}_{\mathrm{SP}} + \mathbf{P}_{\mathrm{R}} \quad (31)$$

with the initial conditions

$$\mathbf{x}_0 = \mathbf{x}(t_0), \quad \dot{\mathbf{x}}_0 = \dot{\mathbf{x}}(t_0), \quad (32)$$

which take into account the effect of the Jupiter gravitational field $\mathbf{P}_{\mathrm{J}}$, the attraction from the Gallilean satellites $\mathbf{P}_{\mathrm{G}}$, from the Sun and planets $\mathbf{P}_{\mathrm{SP}}$ as well as the relativistic effects $\mathbf{P}_{\mathrm{R}}$ within the framework of the Schwartzshield problem. The equations are integrated using the Gauss–Everhart method (Everhart, 1974; Avdyushev, 2006).

The coordinate transformation of $\mathbf{T}$ can be represented as the series of transformations

$$\mathbf{T} = \mathbf{T}_{p_1, p_2} \circ \mathbf{T}_{\mathrm{top}} \circ \mathbf{T}_{\mathrm{geo}}, \quad (33)$$

where $\mathbf{T}_{\mathrm{geo}}$ and $\mathbf{T}_{\mathrm{top}}$ are the transitions from the Jovian center to the geocenter and from the geocenter to the topocenter, respectively; and $\mathbf{T}_{p_1, p_2}$ are the obtained angular coordinates with regard to the observer (topocenter). The transformation of the transition to the topocenter $\mathbf{T}_{\mathrm{top}} \circ \mathbf{T}_{\mathrm{geo}}$ can be formally written as

$$\mathbf{T}_{\mathrm{top}} \circ \mathbf{T}_{\mathrm{geo}}(\mathbf{x}) = \mathbf{x} + \mathbf{x}_{\mathrm{JS}} - \mathbf{x}_{\mathrm{ES}} - \mathbf{x}_{\mathrm{TE}},$$

where $\mathbf{x}_{\mathrm{JS}}$ and $\mathbf{x}_{\mathrm{ES}}$ are the geocentric positions of Jupiter and the Earth, respectively, which are determined from the ephemeris DE405 (Standish, 1998); $\mathbf{x}_{\mathrm{TE}}$ is the geocentric position of the observer calculated by its spherical coordinates: the geocentric distance b, the latitude ψ_{E}, and the local sidereal time s^* as

$$x_{\mathrm{TE1}} = b\cos\psi_{\mathrm{E}}\cos s^*, \quad x_{\mathrm{TE2}} = b\cos\psi_{\mathrm{E}}\sin s^*,$$
$$x_{\mathrm{TE3}} = b\sin\psi_{\mathrm{E}}.$$

Ground-based observations of $\mathbf{p}_i^{\mathrm{O}} = (p_{1i}^{\mathrm{O}}, p_{2i}^{\mathrm{O}})$ are usually related to the moments t_i^{O} of the Greenwich mean time and, thus, when using numerical model (30), it is necessary to preliminarily come to the ephemeris time t_i. In addition, to obtain visible satellite positions $\mathbf{p}_i^{\mathrm{C}} = (p_{1i}^{\mathrm{C}}, p_{2i}^{\mathrm{C}})$ with regard to a ground observer, it is also necessary to take into account the effect of the light lag. Thus, we have the time transformation $t_i = t_i^{\mathrm{O}} + \Delta t_i$, where Δt_i is the correction of the corresponding t_i^{O} for the ephemeris time and the light lag effect.

The components of the six-dimensional vector of initial dynamic state $\mathbf{q} = (\mathbf{x}_0, \dot{\mathbf{x}}_0)$ (32) are the determined parameters (although, theoretically, it is possible to jointly determine all components of the parametric vector $\mathbf{q}^{\mathrm{DT}}$). The parameters are found from the condition of the minimum of functional (26)

$$S(\mathbf{q}) = \frac{1}{2}\sum_{i=1}^{N}[(p_{1i}^{\mathrm{O}} - p_{1i}^{\mathrm{C}})^2 \cos^2 p_{2i}^{\mathrm{O}} + (p_{2i}^{\mathrm{O}} - p_{2i}^{\mathrm{C}})^2].$$

The above composite approach to the minimization of $S(\mathbf{q})$ using iteration schemes (25), (28), and (29) presupposes the calculation of the derivatives $\partial\mathbf{p}^{\mathrm{C}}/\partial\mathbf{q}$. According to (30), they can be represented as

$$\frac{\partial\mathbf{p}^{\mathrm{C}}}{\partial\mathbf{q}} = \frac{\partial\mathbf{T}}{\partial\mathbf{x}}\frac{\partial\mathbf{x}}{\partial\mathbf{q}}. \quad (34)$$

The derivatives $\partial\mathbf{T}/\partial\mathbf{x}$ in dynamic model (30) are obtained analytically from differential correlations

$$\rho^{\mathrm{C}}\mathrm{d}T_1\cos p_2^{\mathrm{C}} = \mathrm{d}x_1\sin p_1^{\mathrm{C}} + \mathrm{d}x_2\cos p_1^{\mathrm{C}},$$

$$\rho^{\mathrm{C}}\mathrm{d}T_2 = \mathrm{d}x_1\cos p_1^{\mathrm{C}}\sin p_2^{\mathrm{C}} + \mathrm{d}x_2\sin p_1^{\mathrm{C}}\sin p_2^{\mathrm{C}} + \mathrm{d}x_3\cos p_2^{\mathrm{C}};$$

while the derivatives $\partial\mathbf{x}/\partial\mathbf{q}$ are found numerically from the differential equations in the variations

$$\frac{\mathrm{d}^2}{\mathrm{d}t^2}\left(\frac{\partial\mathbf{x}}{\partial\mathbf{q}}\right) = \frac{\partial\mathbf{P}}{\partial\mathbf{x}}\frac{\partial\mathbf{x}}{\partial\mathbf{q}} \quad (35)$$

with the initial conditions

$$\left(\frac{\partial\mathbf{x}}{\partial\mathbf{x}_0}\right)_0 = \mathbf{E}, \quad \left(\frac{\partial\mathbf{x}}{\partial\dot{\mathbf{x}}_0}\right)_0 = \mathbf{0},$$

$$\frac{\mathrm{d}}{\mathrm{d}t}\left(\frac{\partial\mathbf{x}}{\partial\mathbf{x}_0}\right)_0 = \mathbf{0}, \quad \frac{\mathrm{d}}{\mathrm{d}t}\left(\frac{\partial\mathbf{x}}{\partial\dot{\mathbf{x}}_0}\right)_0 = \mathbf{E}.$$

Here, $\mathbf{T} = (T_1, T_2)$; ρ is the topocentric distance of the satellite; $\mathbf{x} = (x_1, x_2, x_3)$; and $\mathbf{E}$ is the unitary matrix 3×3 in size. Equations (35) are numerically integrated together with motion equation (31). Thus, during the process of modeling, the system of the 42nd order is integrated. Note that, in this section, we made use of model (30), where, however, the coordinates $\mathbf{x}$ and the derivatives $\partial\mathbf{x}/\partial\mathbf{q}$ were calculated based on the two-body problem formulas.

In the model, Jupiter was considered as a spheroid whose attraction was taken into account with an accuracy up to the sixth zonal harmonic. Formally, the planet attraction can be represented as

$$\mathbf{P}_j = \frac{\partial U}{\partial\mathbf{x}}, \quad \text{where } U = -\mu\sum_i J_i\frac{b_{\mathrm{J}}^i}{|\mathbf{x}|^{i+1}}L_i(\sin\psi_{\mathrm{J}}),$$

$$\sin\psi_{\mathrm{J}} = \frac{x_{\mathrm{J}3}}{|\mathbf{x}|},$$

μ is the gravitational planet parameter; J_i are the coefficients of zonal harmonics, for which $J_0 = -1$; b_{J} is the equatorial Jupiter radius; L_i are Legandre polynomials; and ψ_{J} and $x_{\mathrm{J}3}$ are the latitude and the applicate of the satellite with regard to the planet equator, respectively. The applicate $x_{\mathrm{J}3}$ is determined from the coordinate transformation $\mathbf{x}_{\mathrm{J}} = \mathbf{T}_{\mathrm{J}}\mathbf{x}$ (Seidelmann, et al., 2002), where $\mathbf{T}_{\mathrm{J}}$ is the matrix of the transition from the geoequator to the Jovian equator.

Due to the small dimensions of the gravitating bodies such as Galilean satellites, the Sun, and the planets (except Jupiter) as compared to their distances from inner satellites, they are considered material particles and the attraction of each body in $\mathbf{P}_{\mathrm{G}}$ and $\mathbf{P}_{\mathrm{SP}}$ (31) was calculated by the formula

$$\mathbf{P}_i = \mu_i\left(\frac{\mathbf{x}_i - \mathbf{x}}{|\mathbf{x}_i - \mathbf{x}|^3} - \frac{\mathbf{x}_i}{|\mathbf{x}_i|^3}\right),$$

where μ_i and $\mathbf{x}_i$ are the gravitational parameter and the jovicentric vector of the ith body position. The coordinates of the Galilean satellites were calculated using Lainey theory L1 (Lainey et. al., 2004a; Lainey et.al., 2004b), while the coordinates of the Sun and the planets were computed from the DE405 ephemeris. To optimize the calculations, the orbital parameters of the inner satellites were preliminarily determined using a simplified theory of Galilean satellites, where their positions were calculated using circular motion formulas using the constants from Lieske (1998). Such a stage-by-stage approach allowed for an increase in the speed of the numerical parameter determination by nearly 15 times.

The constants of the Jupiter gravitational field as well as the masses of the Galilean satellites were taken from the Lieske theory E5, while the masses of extraneous planets were taken from DE405.

The relativistic effects were determined within the framework of the Schwartzshield problem using the formula (Brumberg, 1972)

$$\mathbf{P}_{\mathrm{R}} = 4\frac{\mu^2}{c^2|\mathbf{x}|^4}\mathbf{x} + \frac{\mu}{c^2|\mathbf{x}|^3}[4(\mathbf{x}\cdot\dot{\mathbf{x}})\dot{\mathbf{x}} - (\dot{\mathbf{x}}\cdot\dot{\mathbf{x}})\mathbf{x}],$$

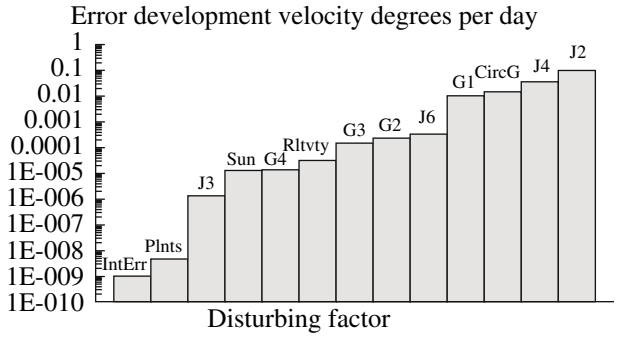

Fig. 10. Velocity of the n^* error distribution in the mean longitude due to ignoring the disturbing factors (Amalthea).

where c is the speed of light.

Figure 10 shows the effect of the disturbing factors on the Almathea orbital motion. The results represented in the figure were obtained through the numerical evaluation of the secular errors in the mean longitude by ignoring these or the above disturbing forces. The results show that the effects of the two first even harmonics of the Jupiter gravitational field (J2, J4) as well as those from the attraction of the most inner Galilean satellite Io (G1) are the most weighty. In particular, already after a ten-year period, the rapid variable perturbation from Jupiterís oblateness becomes on the order of one revolution. The perturbations from the Galilean satellites (G2, G3, G4) decrease with distance from the planet. The effects of the attraction of the Sun and the farthest Galilean satellite Callisto (G4) as well as that of the relativistic effects (Rltvty) are on the same order. The contribution of the perturbations caused by extraneous planets in Amaltheaís motion is the least. Their effect turned out to be so negligible that we decided to completely exclude them from equations (31). In addition, the figure provides the estimates of the perturbations due to the numerical integration errors (IntErr) and the simplification of the orbital model of the Galilean satellites up to a circular one (CircG). It is evident that the influence of the integration errors, as is assumed, is much weaker than the perturbations taken into account. At the same time, the evaluation of CircG shows that the error due to the simplification of the orbital model of giant satellites is so large that the model is totally inadmissible for use in the final processing of observations on inner satellites.

SATELLITE OBSERVATIONS

To determine the orbital satellite parameters, the ground-based observations, whose chronology is given in Table 1, were mainly used. Figure 11 plots the density of the time distribution of the satellite observations. Here, each group of observations is marked with the corresponding code of the observatory (see Table 1); t_0 is the initial point of time at which the orbital parameters were estimated.

It is evident that Amalthea ($N = 707$) and Thebe ($N = 465$) have numerous and sufficient dense observational series. Moreover, the Amalthea observations cover a rather long time interval on the order of 50 years. It should be noted that the majority of all observations for these satellites was obtained at the Itajuba Observatory (Viega, Vieira Martins, 2005) between 1995–2001. In addition, there are several observations from the Hubble Space Telescope (Mallama et al., 2004). All observations made before 1978 are photographic, while later observations were obtained using CCD receivers, and they are represented either in absolute coordinates (p_1, p_2) (A) or in relative coordinates ($\Delta p_1 \cos p_2$, Δp_2), where either Jupiter (J) or one of the Galilean satellites (G) serve as the reference objects.

The amount of observation data on the satellites Adrastea ($N = 90$) and Methis ($N = 178$) are substantially smaller. All of the data were obtained using CCD receivers at two observatories (675 Palomar Mountain and B18 Pik Terskol) and are represented arcsec to Jupiter, the Galilean satellites as well as Amalthea and Thebe (I).

All observation data were taken from the Natural Satellites Data Center Service database http://www.sai.msu.ru/neb/nss/nssnsdcmr.htm (Emelyanov et.al., 2006). Detailed information on the observations used can be found in the papers (Van Biesbroeck, 1955; Sudbury, 1969; Mulholland et.al.,1979; Ianna et.al., 1979; Nicholson, Matthews, 1991; Mulholland et.al., 1979; Viega, Vieira Martins, 1996; Viega, Vieira Martins, 2005; Ledovskaya et.al., 1999; Kulyk et.al., 2002).

To process the relative observations, the coordinates of the reference objects Jupiter and the Galilean satellites were determined from ephemeris DE405 and L1, respectively, while the coordinates of the inner satellites Amalthea and Thebe were calculated using our numerical model (30) based on the parameters obtained using the above observational data.

Due to the small number of satellite observation groups, the problem of the ambiguous determination of the orbital parameters of Adrastea and Metis can occur. Figure 12 plots the functions Φ for each satellite, formally calculated for each observational time. Since the functions Φ are even, they are presented only for $\zeta \geq 0$.

In particular, it is seen that, for Adrastea and Metis, there exist minima of Φ similar in magnitude to the trivial one $\zeta = 0$. This discredits the criterion of the determined parameter quality over the smallness of the target function S, while, as we already know, in the presence of observational errors, the best parameters (those which are the closest to the true ones) do not always return the absolute minimum of the target function, particularly in the case when observations are not numerous. For Metis, there are two such minima: $\zeta/2\pi \approx \pm 11$, while, for Adrastea, many eixst. At the same time, the problem of the ambiguous determination of the orbits is unlikely to occur for Amalthea and Thebe since all

Table 1. Time distribution of the satellite observations

N	Type		Interval (day, month, year–day, month, year)	Observatory
			Amalthea	
41	Photo	A	14.02.1954–22.02.1954	711 McDonald
90	Photo	A	11.01.1967–07.02.1967	88 Kottomia
20	Photo	A	29.09.1976–09.12.1977	711 McDonald
2	Photo	A	17.12.1977	780 Linder MaCormick
10	Photo	A	07.01.1978–09.01.1978	711 McDonald
16	CCD	J	03.12.1988	675 Palomar Mountain
8	CCD	J	15.007.1994–25.08.1994	250 Hubble Space Telescope
203	CCD	A	23.05.1995–14.09.1995	874 Itajuba
2	CCD	J	15.05.1996	250 Hubble Space Telescope
63	CCD	A	21.06.1996–23.08.1996	874 Itajuba
64	CCD	G	26.09.1998–20.11.2000	B18 Pik Treskil
188	CCD	A	25.10.2001–27.10.2001	874 Itajuba
			Thebe	
193	CCD	A	23.05.1995–23.08.1996	874 Itajuba
84	CCD	G	19.09.1998–02.11.1999	B18 Pik Treskil
188	CCD	A	25.10.2001–27.10.2001	874 Itajuba
			Adrsathea	
48	CCD	J	03.12.1988	675 Palomar Mountain
42	CCD	I	05.11.2000–21.11.2000	B18 Pik Treskil
			Metis	
50	CCD	J	03.12.1988	675 Palomar Mountain
128	CCD	G, I	08.10.1999–20.11.2000	B18 Pik Tresko

(nontrivial) minima drastically differ from the trivial one.

Finally, note that the minima Φ for Adrastea increase away from the trivial minimum, although it was shown earlier that, in the case of two observational groups, all minima are equipollent (Fig. 3). This discrepancy is, in reality, explained by the fact that all epochs of the second group of observations (B18 Terskol, Table 1) are distributed over a significant time interval whose duration should not be neglected during careful analysis.

DETERMINATION OF ORBITAL PARAMETERS

Initial estimates of orbital parameters $\mathbf{q}_0$ were preliminarily obtained from observations using the Laplace method. Initial time moments t_0 versus the observational times are given in Fig. 11. In spite of the fact that the fewest stipulations of normal matrices $\mathbf{Q}$ are reached when t_0 is chosen within the interval of moments t_0 for Adrastea and Metis were deliberately left inside the end groups (675 Palomar Mountain), where the observations of the latter are used for obtaining initial estimates of $\mathbf{q}_0$. As indicated earlier using the example of the circular problem, this very choice is convenient for seeking the minima of the target function S in the case of observation groups since the solutions of $\mathbf{q}$ returning the minimum S are close to one another in the phase space of the estimated parameters (Fig. 2).

Using a composite approach with iteration schemes (25), (26), and (29) to minimize $S(\mathbf{q})$ and proceeding

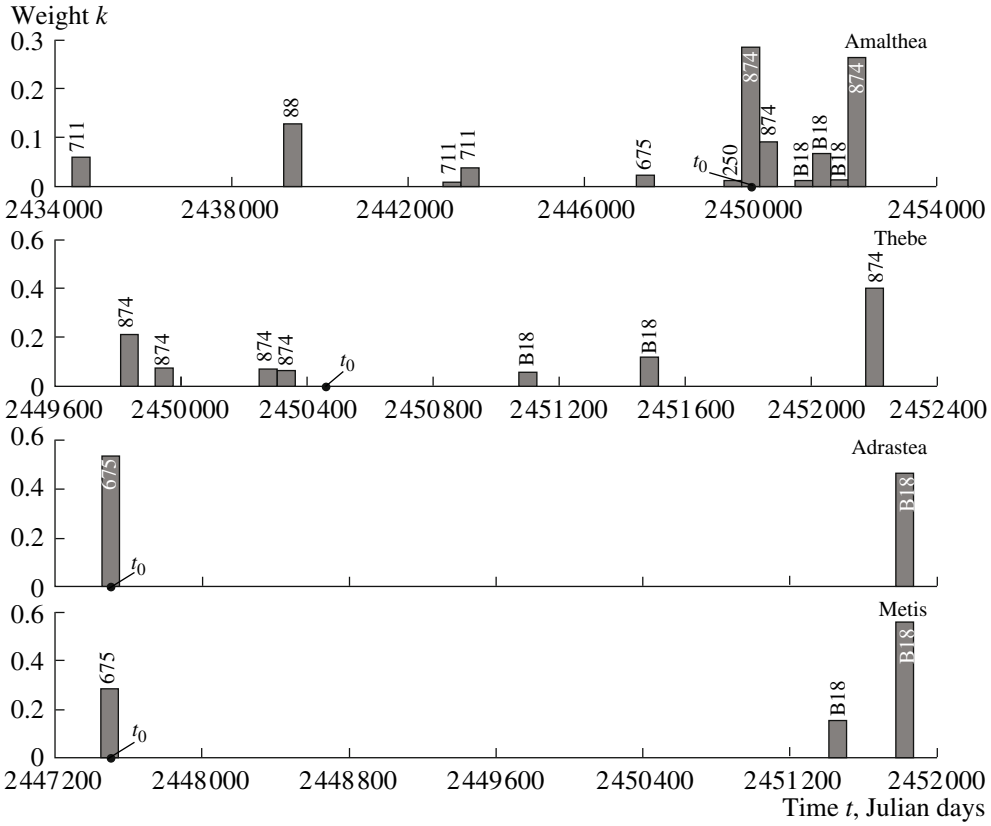

Fig. 11. Time distribution of the satellite observations.

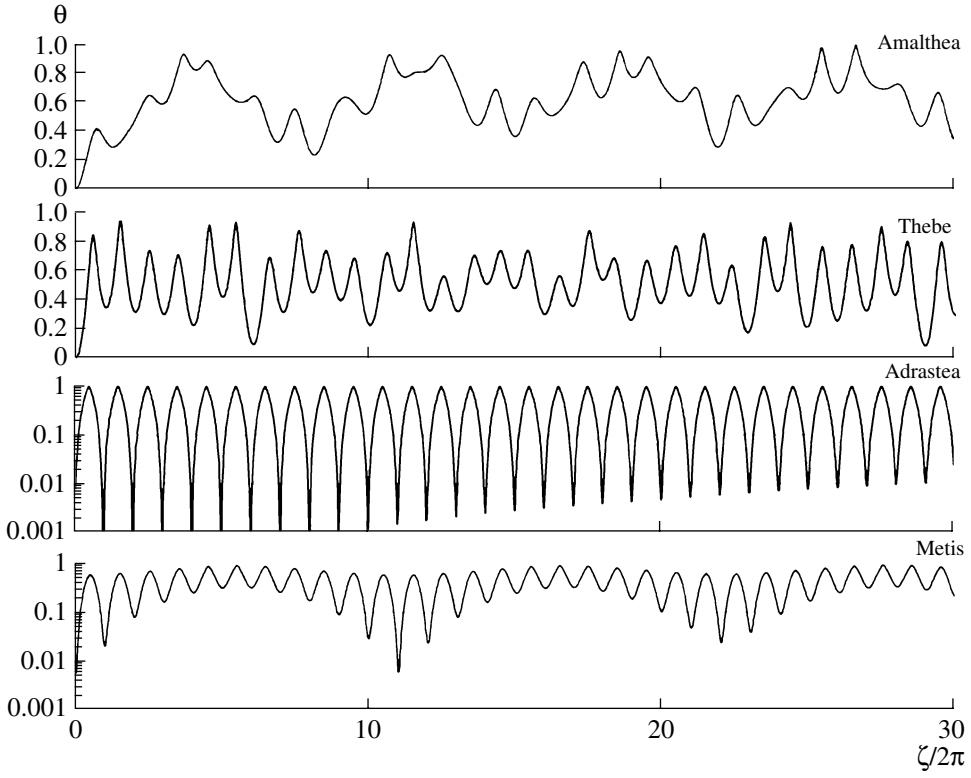

Fig. 12. Behavior of Φ(ζ) for inner satellites.

from initial approximations $\mathbf{q}_0$, over only tens of iterations, we obtained the estimates of orbital parameters $\mathbf{q} = (\mathbf{x}_0, \dot{\mathbf{x}}_0)$ which are given in Table 2. The corresponding orbital elements in their truncated form are given in Table 3. Here, i is the inclination (referred to as the Jupiter equator), τ is the orbital period, and σ_a is the satellite elongation.

The process of fitting a parameter made use of scheme (25) (a gradient descent) until the mean-square error σ converged with an accuracy of up to 0.001″, and, then, scheme (29) (the Gauss–Newton method) was applied. If the corrections in the coordinates $\Delta\mathbf{x}$ exceeded 10^{-7} AU, the solution $\mathbf{q}$ was corrected for its deviation from the energy surface in accordance with scheme (28) (a projection method). Thus, the process continued until all coordinate values reached 10^{-10} AU. All of the limiting values used as a criterion for choosing a specific scheme were selected experimentally. Finally, it should be noted that a well-known Gaussian elimination method was used for the normal matrix inversion in scheme (25).

The obtained parameter estimates return mean-square errors $\sigma = \sqrt{S/N}$ not exceeding 0.4″ (Table 4), which points to a good agreement with the external accuracy of the ground-based observations (Fig. 4 also gives the condition numbers of normal matrices $\mathrm{cond}\mathbf{Q}$ and time intervals Δt and ΔE covering observational times in years and satellite turns, respectively). Discrepancies $\Delta p_1 \cos p_2$ and Δp_2 determining the values of errors σ are given in Figs. 13–16. It should be mentioned that, during the process of parameter determination, some observations whose discrepancy values exceeded 3σ were rejected. Thus, several dozens of such observations were eliminated from the database.

It has already been noted that, to increase the efficiency of the calculations, the orbital parameters were estimated in two stages: first, with a simplified circular model of the Galilean satellites and, then, using the high-accuracy Lainey L1 theory. It is notable, in this connection, that, at both stages, we found nearly the same mean-square errors although the parameters to be determined were principally different. This is because the roughening of the Galilean satellite models within a dynamic model of inner satellites leads mainly to a secular error in the latitude λ^* that actually results in a shift of the target function S along the parameters directly associated with the frequency of the inner satellite revolution, with the minimum values of S being preserved. This has been shown above using the example of a circular problem.

In the result of determining the orbital parameters, we also obtained their covariance matrices $\mathbf{C} = \sigma^2\mathbf{Q}^{-1}$, which are known to describe parametric error distributions. From the practical point of view, the matrices $\mathbf{C}$ can conveniently be represented as

$$\mathbf{C} = \sigma^2\mathbf{W}^T\mathbf{V}\mathbf{W},$$

Table 2. Estimates of the orbital satellite parameters

$\mathbf{x}_0$, Au	$\dot{\mathbf{x}}_0$, AU per day
Amalthea (t_0 = 2449860.5 JD)	
$5.904259045649335\times10^{-4}$	$1.335508654469120\times10^{-2}$
$-9.649762725788387\times10^{-4}$	$6.580573675959994\times10^{-3}$
$-4.443404841108547\times10^{-4}$	$3.311479208243125\times10^{-3}$
Thebe (t_0 = 2450464.5 JD)	
$-6.267081178161467\times10^{-4}$	$1.233321360075275\times10^{-2}$
$-1.230794598107236\times10^{-3}$	$-5.441693601047646\times10^{-3}$
$-5.898550029039168\times10^{-4}$	$-2.105071658282438\times10^{-3}$
Adrastea (t_0 = 2447498.5 JD)	
$-7.303981301488080\times10^{-4}$	$9.634657321571694\times10^{-3}$
$-4.031887607701157\times10^{-4}$	$-1.410217512755373\times10^{-2}$
$-1.986950951223992\times10^{-4}$	$-6.455413514235597\times10^{-3}$
Metis (t_0 = 2447498.5 JD)	
$1.859819984557366\times10^{-4}$	$-1.780689855999936\times10^{-2}$
$7.521256414899649\times10^{-4}$	$3.659703433891211\times10^{-3}$
$3.622658670920554\times10^{-4}$	$1.474969016967715\times10^{-3}$

Table 3. Osculating orbital elements of the satellites

Satellite	$a\times10^3$, AU	e	i, degrees	τ, days	σ_a, ang. vel
Amalthea	1.2165	0.0036	0.3063	0.5016	59.7
Thebe	1.4866	0.0145	1.1248	0.6776	73.8
Adrastea	0.8682	0.0129	0.4613	0.3024	42.1
Metis	0.8615	0.0074	0.0621	0.2989	42.0

Table 4. Statistical data

Satellite	σ, arcsec	N	Δt, years	ΔE, turns	$\log\mathrm{cond}\mathbf{Q}$
Amalthea	0.284	707	47.7	34731	12.9
Thebe	0.161	465	6.4	3467	11.1
Adrastea	0.386	90	12.0	14453	13.1
Metis	0.333	178	12.0	14620	13.5

Table 5. Matrices of **W** for different satellites

Amalthea					
0.8271	0.5494	–0.0916	0.0468	–0.0526	–0.0278
–0.4842	0.7915	0.3644	–0.0694	–0.0342	–0.0172
0.2724	–0.2593	0.9261	0.0161	–0.0251	0.0037
–0.0373	0.0623	0.0287	0.7777	0.5536	0.2875
0.0766	0.0239	0.0131	–0.6218	0.7156	0.3077
0.0009	0.0051	–0.0133	–0.0355	–0.4206	0.9064
Thebe					
0.8998	–0.3920	–0.1250	–0.0152	–0.1296	–0.0635
0.4149	0.8147	0.3904	–0.0977	0.0431	0.0167
–0.0514	–0.4110	0.9101	–0.0051	0.0099	–0.0025
–0.0170	0.1107	0.0588	0.8271	–0.5157	–0.1845
0.1236	–0.0369	–0.0136	0.5507	0.7380	0.3678
0.0016	–0.0061	0.0041	–0.0542	–0.4131	0.9090
Adrastea					
0.8507	0.4697	0.2313	–0.0249	0.0364	0.0167
–0.5225	0.7958	0.3022	0.0304	0.0350	0.0147
–0.0422	–0.3788	0.9245	0.0012	0.0037	–0.0083
0.0396	0.0094	0.0049	0.9078	–0.3958	–0.1322
0.0026	–0.0495	–0.0211	0.4172	0.8473	0.3243
–0.0026	–0.0058	0.0073	–0.0163	–0.3505	0.9364
Metis					
0.9750	–0.2004	–0.0846	–0.0105	–0.0386	–0.0210
0.2172	0.8784	0.4231	–0.0457	0.0094	0.0038
–0.0106	–0.4320	0.9018	–0.0037	–0.0008	0.0039
0.0073	0.0294	0.0141	0.6769	–0.4841	0.5534
0.0448	–0.0056	–0.0018	0.3001	0.8684	0.3922
–0.0026	–0.0272	–0.0191	–0.6704	–0.1001	0.7345

where **W** and **V** are orthogonal and diagonal square matrices, consisting of the directional cosines of the eigenvectors of a normal matrix **Q** and its proper inverse eigenvalues, respectively, which are given in a truncated form in Tables 5 and 6. In particular, as Table 6 shows, a normal matrix (like covariant ones) have greater condition numbers (see also Table 4). This is attributed, first of all, to the fact that the observed data are distributed over long enough time intervals compared to orbital satellite periods τ (Table 3). A connection between the conditionality and the length of the time interval has, in fact, been demonstrated by the example of a circular two-parameter problem, where the matrix determining quadratic form (13) served as a normal matrix:

$$\mathbf{Q} = \begin{pmatrix} \kappa_{11} & \kappa_{12} \\ \kappa_{12} & \kappa_{22} \end{pmatrix}.$$

Comparing formulas (14) and (15), we see that the conditionality of **Q** directly depends of the sum of quadratic deviations on the observational times from the initial epoch. Thus, the best conditionality is reached when choosing an arithmetic mean value for all observational times as the initial epoch.

The ill conditionality of a normal matrix is also known to unfavorably affect its revolution accuracy (mainly due to the strong rounding up errors) and, as a result, the convergence of the Gauss–Newton iteration scheme. Nevertheless, in our case, the conditional numbers turn out not to be large enough to significantly affect the quality of the normal matrix inversion.

OTHER ESTIMATES

In spite of the smallness of the mean-square errors for Adrastea and Metis (Table 4), other minima of the functional S exist, where the errors take on close values. (Like below, weíll consider a set of different solutions returning minima of S; for the sake of convenience, all of the variables related to the above estimates of the orbital parameters will be marked with a tilde). To find these minima, in accordance with (17), we varied the values of the total energy H with the step $\Delta H = 2\tilde{H}/3\tilde{R},$; then, according to scheme (29), we found

Table 6. Components of the diagonal matrices **V** (proper numbers $\mathbf{Q^{-1}}$)

Satellite	v_1	v_2	v_3	v_4	v_5	v_6
Amalthea	5.259×10^{-2}	5.709×10^{-12}	5.008×10^{-2}	6.595	48.56	12.23
Thebe	4.237×10^{-2}	4.61×10^{-10}	9.838×10^{-2}	7.339	47.96	8.202
Adrastea	9.023×10^{-11}	0.183	0.505	1092	483.5	167.7
Metis	0.128	1.823×10^{-11}	0.222	76.81	511.8	79.14

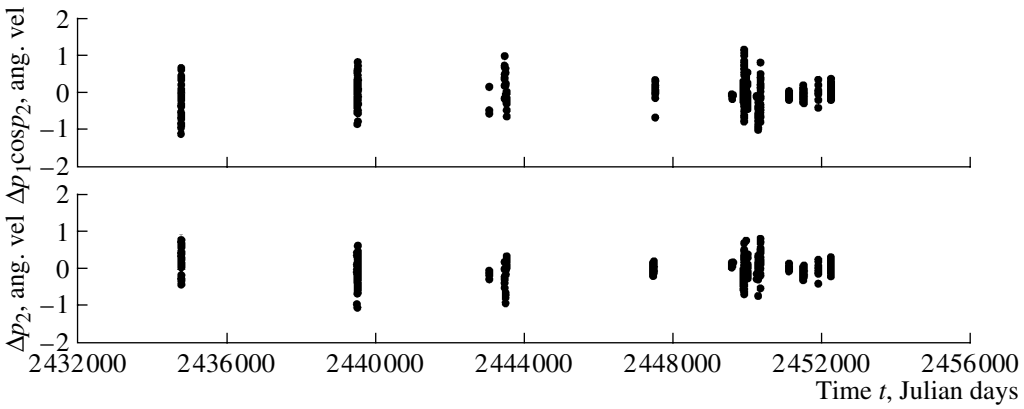

Fig. 13. Model discrepancy for Amalthea.

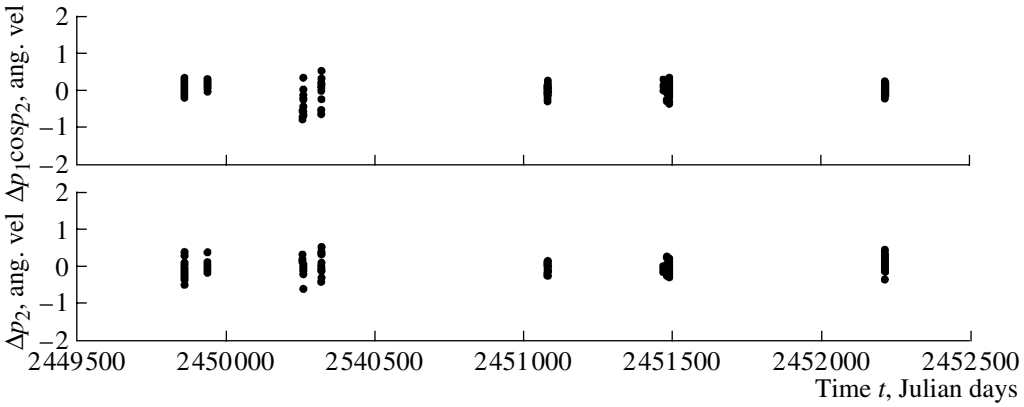

Fig. 14. Model discrepancy for Thebe.

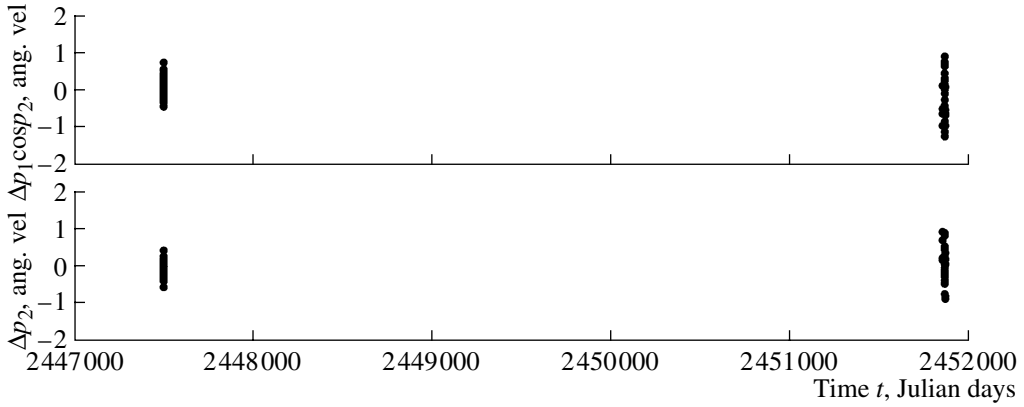

Fig. 15. Model discrepancy for Adrastea.

approximate values of the parameters $\mathbf{q}_0$ and, finally, using each $\mathbf{q}_0$ approximation, we performed the parameter improvement procedure described above. In total, 50 neighboring solutions were analyzed for Adradthea, while, for Metis, we considered only the two corresponding to the minima $\zeta/2\pi \approx \pm 11$ of the function $\Phi(\zeta)$ (Fig. 12).

It is particularly remarkable that, for Adrastea, the absolute minimum of the mean-square error is reached just at the solution $\tilde{\mathbf{q}}$ (Table 2). However, other minima

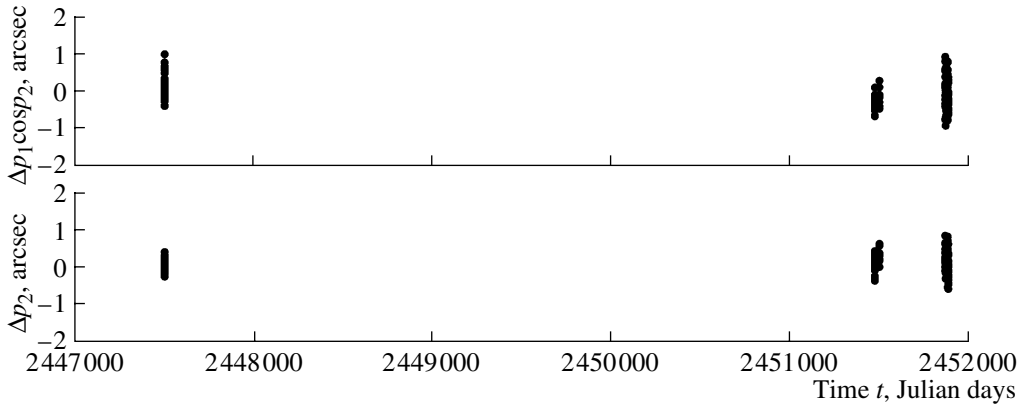

Fig. 16. Model discrepancy for Metis.

close to σ exist in its neighborhood whose values differ from $\tilde{\sigma}$ by less than 0.01″ (Fig. 17). Thus, we have sufficient evidence to suspect that the best (in terms of being the closest to the true parameters) estimates can, with a high degree of probability, be found in the neighboring minima.

Needless to say, there is a temptation to attract some additional a priori information on the satellite orbits to single out the best estimates from among those presented. For example, taking into account that the satellite orbits are nearly circular or equatorial, we can chose from all $\mathbf{q}$ those which correspond to the least eccentricity or inclination. However, as has been shown using the example of a two-body problem (Fig. 7), rather good orbital elements from the a priori point of view can be given by estimates, which are far from the true parameters.

Figures 18–20 show the distribution of solutions in the orbital components along H. The initial solution of $\tilde{\mathbf{q}}$ given in Table 2 is marked in the figures with a ring. In particular, if we compare Figs. 17 and 19, we can see that the least eccentricity ($e = 8 \times 10^{-4}$) corresponds to the mean-square error (σ = 0.87″), which is far from being the best. However, the same situation is observed for the inclination ($i = 0.18°$, σ = 0.64″) (Fig. 20).

As for Metis, the results of the investigation of two suspicious solutions once and for all destroyed all doubts concerning their belonging to potentially acceptable solutions for the description of a satellite orbit: the data in Table 7 show that mean-square error of adjacent solutions is significantly larger than the error of the initially obtained solution $\tilde{\mathbf{q}}$ (Table 4). In addition, it is worth noting that both the eccentricity and the inclination for $\tilde{\mathbf{q}}$ take on the lowest values (Table 3).

Taking advantage of the fact that we have three observation groups for Metis (Fig. 11), we carried out a very interesting experiment whose results vividly demonstrate the importance of the problem of ambiguous orbit determinations in the view of planning future satellite observations. We determined the orbital parameters based on two observation groups (675 Palomar Mountain, B18 Pik Terskol) between 1988ó1999, and, then, to forecast satellite positions at the observational times of the third group.

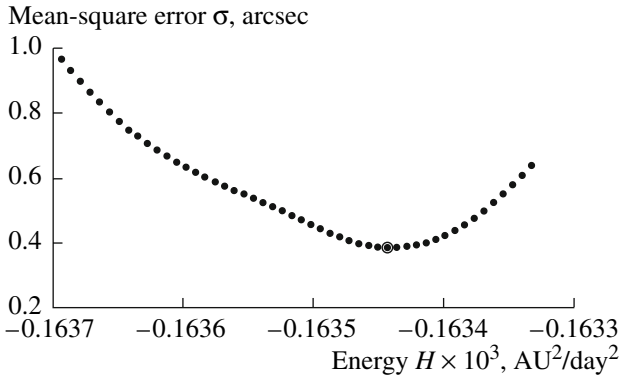

Fig. 17. Mean-square errors for different solutions (Adrastea).

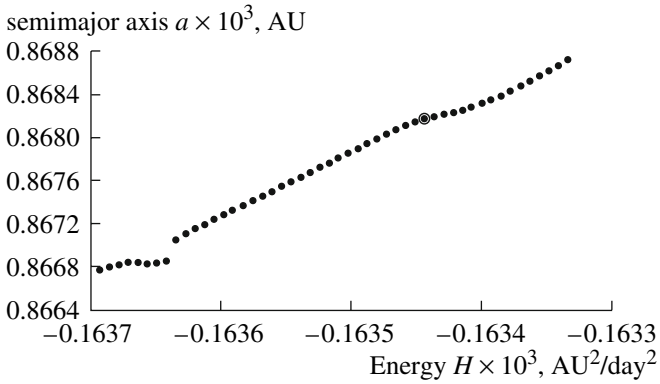

Fig. 18. Values of the semimajor axis for different solutions (Adrastea).

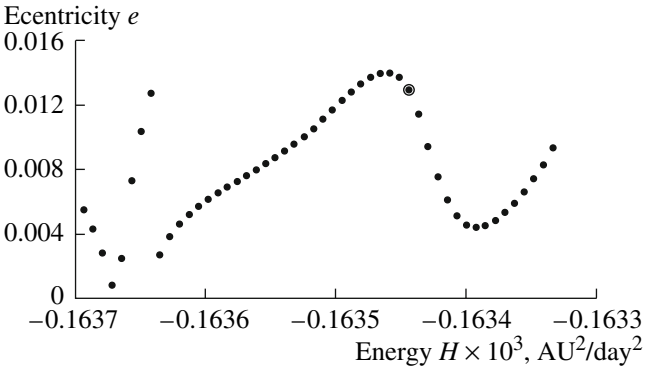

Fig. 19. Eccentricity values for different solutions (Adrastea).

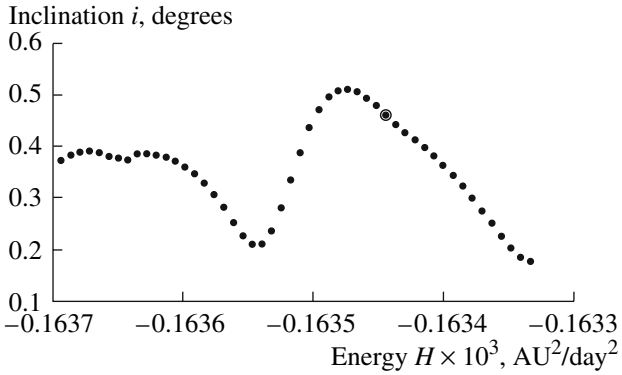

Fig. 20. Inclination values for different solutions (Adrastea).

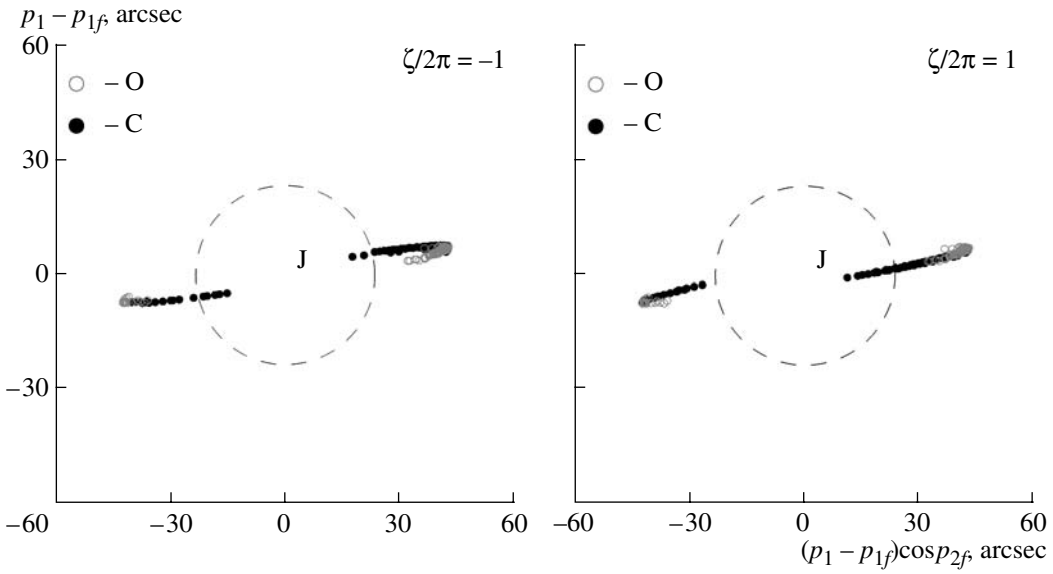

Fig. 21. Distribution of the observed (O) and calculated (C) positions of Metis in the coelosphere for the third group of observations (B18 Pik Treskol) (the dashed lines show the boundary of the Jupiter disc visible from the Earth).

Using the data of two groups, we can find a set of solutions for **q** that minimize the target function S; but, we considered only the three adjacent to $\zeta/2\pi = -1, 0, 1$ (a zero solution corresponds to $\tilde{\mathbf{q}}$). The orbital components for these solutions are given in Table 8. It should be noted that minimal mean-square errors σ takes place for $\zeta/2\pi = 1$, although, as we know from the results of the orbit determination based on three observational groups, the best parameter estimate is for $\zeta/2\pi = 0$.

The coelosphere positions of the satellite (C) modeled on the basis of two adjacent solutions for the third group of observations (O) are given in Fig. 21. It is clearly seen that a numerical forecast of the satellite elongation is rather rough. Thus, using a dynamical model of the object to plan its observations at any other precalculated elongation moment, not only will we be unable to find it at an expected location, we may not be able to observe it at all because it is likely to be in front of Jupiter, behind it, or nearby it blinded out by light coming from the planet. Other adjacent solutions will evidently give a rougher forecast.

COMPARISON WITH JUP230 EPHEMERIS

Simulation results were compared with JUP230 ephemeris (Jacobson, 1994), which are available at the website of the Jet Propulsion Laboratory (JPL NASA): http://ssd.jpl.nasa.gov/horizons.cgi. Using JUP230

Table 7. Orbital elements of Metis and the mean-square errors for adjacent solutions

$\zeta/2\pi$	$a \times 10^3$, AU	e	i, degrees	τ, days	σ, arcsec
−11	0.8618	0.0120	0.2002	0.2991	0.987
11	0.8609	0.0101	0.2325	0.2986	1.119

Table 8. Orbital elements of Metis and mean-square errors for adjacent solutions for the case of two observational groups

$\zeta/2\pi$	$a\times10^3$, AU	e	i, degrees	τ, days	σ, ang. vel
–1	0.8615	0.0069	0.1933	0.2990	0.280
0	0.8615	0.0100	0.1682	0.2990	0.257
1	0.8615	0.0132	0.1488	0.2990	0.245

Table 9. Mean-square deviations of the ephemeris and osculating orbital elements of satellites obtained for JUP230

Satellite	σ, arcsec	σ_{jac}, ang.vel.	$a_{jac}\times\times10^3$, AU	e_{jac}	i_{jac}, degrees	τ_{jac}, days
Amalthea	0.076	0.035	1.2165	0.0036	0.3817	0.5016
Thebe	0.217	0.037	1.4865	0.0160	1.0845	0.6776
Adrastea	0.272	0.036	0.8681	0.0065	0.0096	0.3024
Metis	0.168	0.039	0.8615	0.0071	0.0043	0.2989

ephemeris, in the 20-year time interval from 1980 to 2000, we generated the observations of inner satellites with a 30-day interval. Based on these observations, we estimated a mean-square error σ of our model with $\tilde{\mathbf{q}}$ parameters (Table 2) and, then, fitted those parameters to the observations generated. The results are given in Table 9. Here, the index *jac* denotes the values obtained in the result of the numerical model adjustment to JUP230 ephemeris.

It should be immediately noted that the solution of $\tilde{\mathbf{q}}$ for Adrastea showed a poor agreement with JUP230. We checked the adjacent solutions and it turned out that JUP230 ephemeris is in good agreement with the solution corresponding to $\zeta/2\pi = -1$. The table shows the estimates for this very solution. Hence, we would not hurry to state that this solution is the best estimate of the orbital parameters.

As far as we know, not only ground-based observations but also spacecraft observations were used for constructing JUP230 ephemeris. Thus, there should seemingly be no peculiarities associated with the ambiguity of the orbital determination when constructing the ephemeris. Nevertheless, we cannot say it with certainty until this problem is given a thorough consideration.

Thus, coming back to Table 9, we see that our results for Amalthea are in very good agreement with the NASA ephemeris, while those for other satellites are a bit worse. This is explained by the fact that, for a satellite known for many years, the number of observation data covering a longer time interval is larger than that for satellites discovered only in 1979. An increase in the time interval of uniformly precise observations is known to decrease the degree of uncertainty in the parameters estimated based on observations. Nevertheless, in spite of the large mean-square errors for Thebe, Adrastea, and Metis, they remain within the external accuracy of the ground-based observations.

After the model was adjusted to JUP230 ephemeris, we found sufficient small mean-square values of σ_{jac} on the order of $0.04''$ (Table 9) probably due to the fact that they are associated with the absence of short-period perturbations as the positions of satellites in JUP230 are calculated using the formulas of the precessing ellipsis (Jacobson, 1994). Hence, the satellite periods did not change significantly, which cannot be said about the eccentricities and inclinations, especially for Adrastea and Metis; the values of these components decreased. However, the above does not give us grounds to make any conclusions on the quality of NASA ephemeris, since the model underlying it is principally different from ours.

CONCLUSIONS

To conclude, let us summarize the key results of this work.

1. The problem of the ambiguous orbit determination that frequently occurs in the inverse problems of the inner satellite dynamics when their orbits are determined based on several observation groups distributed over rather long time intervals has been formulated.

2. The problem of the ambiguity in orbit determination has been studied in detail by the example of a two-body circular problem. In particular, the unpleasant peculiarity considered in inverse problems is shown to become most relevant when two groups of observations are distributed at the extremities of the time interval; under these circumstances, the target function has a set of nearly equipollent minima and the choice for the best solutions from among those where the minima are reached becomes practically impossible, in particular, when there are very few observations containing large errors. The problem can occur at a so-called resonant distribution of the observational groups, this being one of the favorable conditions for the appearance of nearly equipollent target function minima.

3. The characteristic Φ graphically demonstrating the approximate distributions of the target function minima along the parameter directly linked with the frequency of the satellite revolution has been introduced. This characteristic is convenient for studying inverse problems with the object of finding a set of solutions.

4. Using the example of a circular problem, the ravine shape of a minimized function (the conditionality of the matrix of an approximate quadratic form) has been shown to directly depend of the sum of the quadratic deviations of observational times with regard to the initial epoch. This implies that the lowest degree of ravinity (the best conditionality) is reached when a normal value of all observational times is chosen as the initial epoch.

5. The capabilities of the Gauss–Newton method as applied to the dynamic model based on two-body problem formulas have been studied. Numerous experiments have shown that the method has a low efficiency for the considered inverse problems. In particular, the convergence domain of the iteration Gauss–Newton scheme is so small that, from the applied point of view, it is absolutely useless to use this scheme. In this connection, we have suggested a composite approach to the orbital parameter determination, which would allow one to quickly find the target function minimum even when the initial approximations are rather rough. This approach assumes the use of thewell-known gradient descent method and the so-called projection method to modify the Gauss–Newton scheme.

6. A numerical model of the inner satellite orbital motions taking into account the key disturbing factors such as the nonspherical character of the Jupiter gravitational field (up to the sixth zonal harmonic), the attraction of the Galilean satellites, the Sun, and extraneous planets as well as the relativistic effects within the framework of the Schwatzshield problem, has been constructed.

7. Based on the available observational data on the satellites (Amalthea, Thebe, Adrastea, and Metis), their orbital parameters as well as the corresponding covariance matrices which characterize the distribution of the parametric errors have been obtained.

8. Adjacent estimates of the Adrastea and Metis orbital parameters have been studied in the view of their belonging to those which are potentially acceptable for describing the satellite orbits. Due to the fact that Adrastea has two observational groups, it turns out to be impossible to get reliable estimates of the orbital satellite parameters. At the same time, in spite of the fact that Metis has also been observed infrequently, we have no doubts that initially obtained estimates of the orbital parameters are best and can be recommended for the numeric modeling of the satellite orbit.

We note, finally, that all of the theoretical results obtained in this paper can be generalized for any satellite system. For example, the problem of the ambiguous determination of the orbits will, at least, take place when a set of solutions along the parameter associated with the satellite revolution frequency are within the area of its legitimate values. If the semimajor axis a is taken as such a parameter, and $\delta a = a\sigma/\sigma_a$ is the limiting variation, then, in accordance with (17), for two observational groups, a set of solutions can be obtained, if

$$R > \frac{3}{2}\frac{\sigma_a}{\sigma},$$

where R is the number of satellite revolutions which keep within the time interval specified by the observations, σ_a is the satellite elongation, and σ is a typical value for the observational errors.

ACKNOWLEDGMENTS

The authors thank Prof. A.M. Chernitsova and Prof. T.V. Bordovitsina for their participation in discussions of the results and valuable remarks and suggestions. This work was supported by the Russian Foundation for Basic Research (project no. 05-02-17043).

REFERENCES

Avdyushev, V.A., Gauss-Everhart's Integrator. New FORTRAN-Cod, *Materialy vseross. konf. "Fundamental'nye i prikladnye problemy sovremennoi mekhaniki"* (Proc. All-Russian Conf. "Fundamental and Applied Problems of Modern Mechanics"), Tomsk: Tomsk. Gos. Univ., 2006, pp. 413-414.

Arazov, G.T., Analytical Theory of the Motion of the Fifth Satellite of Jupiter, *Izv. Akad. Nauk AzSSR, Ser. Fiz.-Tekh. Mat. Nauk*, 1972, vol. 2, pp. 75–81.

Attetkov, A.V., Galkin, S.V., and Zarubin, V.S., *Metody optimizatsii* (Optimization Methods), Moscow: MGTU, 2001.

Ban'shchikova, M.A. and Avdyushev, V.A., Chislennoe modelirovanie dinamiki sputnikov Yupitera, *Izv. Vyssh. Uchebn. Zaved., Fiz. Prilozh. "Nebesnaya Mekh. Prikl. Astron."*, 2006, vol. 49, no. 2, pp. 74–82.

Barnard, E.E., Discovery and Observations of a Fifth Satellite to Jupiter, *Astron. J.*, 1892, vol. 12, no. 11, pp. 81–85.

Breiter, S., The Theory of Motion of JV Amalthea, *Astron. Astrophys.*, 1996, vol. 314, pp. 966–976.

Brumberg, V.A., *Relyativistskaya Nebesnaya Mekhanika* (Relativistic Stellar Mechanics), Moscow: Nauka, 1972.

Chernitsov, A.M., Analysis of Some Simplified Schemes of Estimate of the Parameters of Motion of Celestial Bodies, *Astron. Geodez.*, 1975, no. 5, pp. 6–19.

Cohn, F., Bestimmung der Bahnelemente des V. Jupitersmondes, *Astron. Nachr.*, 1897, vol. 142, pp. 289–338.

Emel'yanov, N.V., Arlo, Zh.Yu., Varfolomeeev, M.I., et al., Construction of Theories of Motion, Ephemerides, and Databases for Natural Satellites of Planets, *Kosm. Issled.*, 2006, vol. 44, pp. 136–145 [*Cosmic. Res.* (Engl. Trasnl.), vol. 44, pp. 128–136].

Escobal, P., *Methods of Orbit Determination*, New York: Wiley, 1965, p. 463.

Everhart, E., Implicit Single Sequence Methods for Integrating Orbits, *Celest. Mech.*, 1974, vol. 10, pp. 35–55.

Himmelblau, D.M., *Applied Nonlinear Programming*, Austin: The University of Texas, 1972.

Ianna, P.A., Seitzer P., and Levinson, F., Astrometric Observations of the Satellites of the Outer Planets. I – The Galilean Satellites in 1977, *Astron. J.*, 1979, vol. 84, pp. 429–435.

Jacobson, R.A., Revised Ephemerides of the Inner Jovian Satellites, *JPL IOM*, 1994, vol. 314, pp. 10-101.

Jewitt, D.C., Danielson, G.E., and Synnott, S.P., Discovery of a New Jupiter Satellite, *Science*, 1979, vol. 206, pp. 951.

Kiryushenkov, V.N., Analytical Theory of the Motion of the Fifth Satellite of Jupiter, *Cand. Sci. (Phys-Math.) Dissertation,* Moscow: Mosk. Gos. Univ., 1969.

Kulyk, I., Jockers, K., Karpov, N., and Sergeev, A., Astrometric CCD Observations of the Inner Jovian Satellites in 1999-2000, *Astron. Astrophys.*, 2002, vol. 383, pp. 724-728.

Lainey, V., Duriez, L., and Vienne, A., New Accurate Ephemerides for the Galilean Satellites of Jupiter. I. Numerical Integration of Elaborated Equations of Motion, *Astron. Astrophys.*, 2004a, vol. 420, pp. 1171–1183.

Lainey, V., Arlot, J.E., and Vienne, A., New Accurate Ephemerides for the Galilean Satellites of Jupiter. II. Fitting the Observations, *Astron. Astrophys.*, 2004b, vol. 427, pp. 371–376.

Ledovskaya, I.V., Iokers, K., Karpov, N.V., and Sergeev, A.V., Astrometric CCD Observations of Jupiter's Inner Satellites Thebe and Amalthea and Saturn's Satellite Phoebe in the 1998 Opposition, *Kinematika Fiz. Nebesnykh Tel*, 1999, vol. 15, no. 6, pp. 483–488.

Lieske, J., Galilean Satellites Ephemerides E-5, *Astron. Astrophys.*, 1998, vol. 129, pp. 205–217.

Mallama, A., Aelion, M., and Mallama, C.A., Jovian Satellite Positions from Hubble Space Telescope Images, *Icarus*, 2004, vol. 167, no. 2, pp. 320–329.

Mulholland, J.D., Benedict, G.F., and Shelus, P.J., Absolute and Relative Positions of Jupiter V (Amalthea) and the Galilean Satellites 1976-1978, *Astron. J.*, 1979, vol. 84, pp. 668-670.

Nicholson, P.D. and Matthews, K., Near-Infrared Observations of the Jovian Ring and Small Satellites, *Icarus*, 1991, vol. 93, pp. 331-346.

Pascu, D., Astrometric Techniques for the Observation of Planetary Satellites, *Planetary Satellites*, Tucson: Univ. of Arizona Press, 1977, pp. 63-86.

Seidelmann, P.K., Abalakin, V.K., Bursa, M., et al., Report of the IAU/IAG Working Group on Cartographic Coordinates and Rotational Elements of the Planets and Satellites: 2000, *Celest. Mech.*, 2002, vol. 82, no. 1, pp. 83–111.

Standish, E.M., JPL Planetary and Lunar Ephemerides, DE405/LE405, *Interoffice Memorandum*, 1998, vol. 312, F-98-048, pp. 1–18.

Sudbury, P.V., The Motion of Jupiter's Fifth Satellite, *Icarus*, 1969, vol. 10, pp. 116–143.

Synnott, S.P., Orbits of the Small Inner Satellites of Jupiter, *Icarus*, 1984, vol. 58, pp. 178–181.

Tisserand, M.F., Sur le mouvement du cinquieme satellite de Jupiter, *Comptes rendus hebdomadaires des seances de l'Academie des sciences*, France: Academie des sciences, 1893, vol. 117, pp. 1024–1027.

Van Biesbroeck, G., Observations of Jupiter's Fifth Satellite, *Astron. J.,* 1955, vol. 60, p. 275.

Van Woerkom, A.J.J., The Motion of Jupiter's Fifth Satellite, 1892-1949, *Astronomical Papers Prepared for the use of the American Ephemeris and Nautical Alamanac*, 1950, vol. 13, pp. 1–77.

Veiga, C.H., Vieira Martins R. Astrometric observations of Amalthea and Thebe *Rev. Mex. de Astron. y Astrofis. Ser. de Conf., VIII Reunion Regional Latino Americana de Astronomia Union Astronomica Internacional*, (Montevideo, Uruguay, 1995), 1996, vol. 4, pp. 118.

Veiga, C.H., Vieira Martins, R., CCD Astrometric Observations of Amalthea and Thebe, *Astron. Astrophys.,* 2005, vol. 437, no. 3, pp. 1147–1150.